Plasmid construction

The expression construct, including mouse *Braf* cDNA, was purchased from Origene (Rockville, MD, USA). PCR was performed using primers designed to introduce *Hin*dIII sites and the V5 epitope (C terminus). The PCR fragment was subcloned into pCR4-TOPO Vector (Invitrogen). The entire cDNA was verified by sequencing. The mutant constructs for *Braf* Q241R and V637E were generated using QuikChange Lightning Site-Directed Mutagenesis Kit (Stratagene, La Jolla, CA, USA) with the primers, 5′-CCGAAAGCTGCTTTTCCGGGGTTT CCGTTGTCAAA-3′ and 5′-TTTGACAACGGAAACCCCGG AAAAGCAGCTTTCGG-3′, and 5′-CTTTGGTCTAGCCACA GAGAAATCTCGGTGGAGTG-3′ and 5′-CACTCCACCGA GATTTCTCTGTGGCTAGACCAAAG-3′, respectively. All mutant constructs were verified by sequencing. The cDNAs were digested with *Hin*dIII, blunt-ended with T4 DNA polymerase and ligated into blunt-ended *Eco*RI site of pCAGGS vector (50).

Reporter assay

NIH 3T3 cells (ATCC, Rockville, MD, USA) were maintained in Dulbecco's modified Eagle's medium supplemented with 10% newborn calf serum, 50 U/ml penicillin and 50 μg/ml of streptomycin. The cells were seeded in 24-well plates at 3×10^5 cells/well 24 h before transfection. The cells were then transiently transfected using Lipofectamine and PLUS Reagent (Invitrogen) with 400 ng of pFR-luc, 25 ng of pFA2-Elk1, 5 ng of phRLnull-luc and 5 ng of WT or mutant expression constructs of *Braf*. Forty-eight hours after transfection, the cells were harvested in passive lysis buffer, and luciferase activity was assayed using Dual-Luciferase Reporter Assay System (Promega). Renilla luciferase expressed by phRLnull-luc was used to normalize the transfection efficiency.

Western blotting and phospho-kinase-antibody array

Whole-mouse embryos and brain were lysed in lysis buffer (10 mM Tris–HCl, pH 8.0 and 1% SDS), or genotype-confirmed hearts were pooled and lysed in the same buffer. These lysates were centrifuged at 14 000*g* for 15 min at 4°C and the protein concentration was determined by the Bradford method with Bio-Rad Protein Assay (Bio-Rad Laboratories, Hercules, CA, USA). Lysates were subjected to SDS–polyacrylamide gel electrophoresis (5–20% gradient gel; ATTO, Tokyo, Japan) and transferred to nitrocellulose membrane. Antibodies used were as follows (with catalog numbers in parentheses): B-RAF (9434), ERK1/2 (9102), phospho-ERK1/2 (9101), phospho-MEK (9121), p38 (9212), phospho-p38 (4511), phospho-SAPK/JNK (4668), AKT (9272), phospho-AKT (on Ser473; 9018) and phospho-AKT (on Thr308; 2965) from Cell Signaling (Danvers, MA, USA). C-RAF (610152), MEK (sc-219) and β-actin (A5316) were from BD Transduction Laboratories (San Jose, CA, USA), Santa Cruz Biotechnology (Santa Cruz, CA, USA) and Sigma-Aldrich, respectively. All the membranes were visualized using Western Lightning ECL-Plus Kit (Perkin-Elmer, Waltham, MA, USA). The band intensities were quantified using ImageJ software (http://rsbweb.nih.gov/ij/) and normalized to β-actin. Phosphorylated protein was measured to determine the ratios of phosphorylated protein to non-phosphorylated protein and then normalized to β-actin.

For kinase-antibody arrays, protein extracts of embryonic hearts (400 μg) were incubated with the Phospho-Kinase Antibody Array Kit (Proteome Profiler Antibody Array; R&D systems, Minneapolis, MN, USA) following the manufacturer's instructions.

Histology and immunohistochemistry

Embryonic hearts were perfused with phosphate-buffered saline and 10% neutral buffered formalin from the placenta. The fixed hearts and whole-mouse embryos fixed in 10% neutral buffered formalin were embedded in paraffin. Embedded tissues were sectioned at 6 μm (hearts) or 3 μm (whole-mouse embryos and lungs). Sections were stained with hematoxylin and eosin. In hearts from embryos at E16.5, the largest diameters of the ventricular radius were measured in serial coronal sections where a four-chamber view was observed. The largest thicknesses of cardiac valve leaflets in serial sections were measured. Edematous and dead embryos were excluded from these analyses.

For immunohistochemistry, the antibodies used were as follows (with catalog numbers in parentheses): phospho-Histone H3 (9701) from Cell Signaling, LYVE-1 (103-PA50AG) from RELIA Tech GmbH (Braunschweig, Germany), α-SMA (M0851) from DAKO (Glostrup, Denmark), PECAM-1 (CD31; sc-1506) from Santa Cruz Biotechnology and TTF-1 (MS-669-P1ABX) from Thermo Fisher Scientific (Fremont, CA, USA). Signals were amplified by Histofine Simple Stain (Nichirei Bio Sciences, Tokyo, Japan) and color was developed by DAB Substrate Kit (Nichirei Bio Sciences). Sections were counterstained with hematoxylin.

PAS staining

Deparaffinized lung sections were incubated in 0.5% periodic acid for 10 min at 60°C, rinsed with distilled water and stained in Schiff's reagent (Muto Pure Chemicals, Tokyo, Japan) for 10 min. Stained slides were counterstained with hematoxylin, dehydrated and mounted.

Animal treatment

Stock solution of PD0325901 (Sigma-Aldrich) was prepared using ethanol, whereas those of MAZ-51 (Calbiochem, San Diego, CA, USA), Sorafenib (Toronto Research Chemicals, North York, ON, USA), Lovastatin (Calbiochem), Everolimus (Selleckchem, Houston, TX, USA), NCDM-32b (Wako Pure Chemicals, Osaka, Japan), GSK-J4 (Cayman Chemical) and the combination of PD0325901 and GSK-J4 were prepared using dimethylsulfoxide. PD0325901 was resuspended in saline while and all other reagents were resuspended in 0.5% hydroxypropylmethylcellulose with 0.2% Tween80, respectively. The prepared reagents or vehicles were i.p. injected into pregnant mice daily, beginning on E10.5 and continuing till E15.5 or E18.5.

Statistical analysis

All statistical analysis was performed using Prism software (ver. 6.01; GraphPad Software, Inc., San Diego, CA, USA). Data analysis were performed with Student's *t*-test for unpaired samples, one-way analysis of variance followed by the Tukey–Kramer test for comparison of multiple experimental groups and the χ^2 test for differences between observed and expected distributions. Differences were considered significant at a *P*-value of < 0.05.

SUPPLEMENTARY MATERIAL

Supplementary Material is available at *HMG* online.

ACKNOWLEDGEMENTS

We are grateful to Jun-ichi Miyazaki, Osaka University, for supplying the pCAGGS expression vector. We thank Riyo Takahashi, Kumi Kato, Yoko Tateda and Daisuke Akita for technical assistance and Fumiko Date for technical assistance and for discussion of the experimental data. We also acknowledge the support of the Biomedical Research Core of Tohoku University Graduate School of Medicine. We thank RIKEN BioResource Center for providing us with B6.Cg-Tg(CAG-Cre)CZ-MO2Osb mice (RBRC01828).

Conflict of Interest statement. None declared.

FUNDING

This work was supported by the Funding Program for the Next Generation of World-Leading Researchers (NEXT Program) from the Ministry of Education, Culture, Sports, Science and Technology of Japan to Y.A. (LS004), by Grants-in-Aids from the Ministry of Education, Culture, Sports, Science and Technology of Japan, the Ministry of Health, Labor and Welfare, and the Japan Society for the Promotion of Science (JSPS) KAKENHI Grant number 26293241 to Y.A., and by JSPS KAKENHI Grant number 25860839 to S.I.

REFERENCES

1. Reynolds, J.F., Neri, G., Herrmann, J.P., Blumberg, B., Coldwell, J.G., Miles, P.V. and Opitz, J.M. (1986) New multiple congenital anomalies/mental retardation syndrome with cardio-facio-cutaneous involvement – the CFC syndrome. *Am. J. Med. Genet.*, **25**, 413–427.
2. Witters, I., Denayer, E., Brems, H., Fryns, J.P. and Legius, E. (2008) The cardiofaciocutaneous syndrome: prenatal findings in two patients. *Prenat. Diagn.*, **28**, 53–55.
3. Niihori, T., Aoki, Y., Narumi, Y., Neri, G., Cave, H., Verloes, A., Okamoto, N., Hennekam, R.C., Gillessen-Kaesbach, G., Wieczorek, D. *et al.* (2006) Germline KRAS and BRAF mutations in cardio-facio-cutaneous syndrome. *Nat. Genet.*, **38**, 294–296.
4. Rodriguez-Viciana, P., Tetsu, O., Tidyman, W.E., Estep, A.L., Conger, B.A., Cruz, M.S., McCormick, F. and Rauen, K.A. (2006) Germline mutations in genes within the MAPK pathway cause cardio-facio-cutaneous syndrome. *Science*, **311**, 1287–1290.
5. Narumi, Y., Aoki, Y., Niihori, T., Neri, G., Cave, H., Verloes, A., Nava, C., Kavamura, M.I., Okamoto, N., Kurosawa, K. *et al.* (2007) Molecular and clinical characterization of cardio-facio-cutaneous (CFC) syndrome: overlapping clinical manifestations with Costello syndrome. *Am. J. Med. Genet. A*, **143A**, 799–807.
6. Abe, Y., Aoki, Y., Kuriyama, S., Kawame, H., Okamoto, N., Kurosawa, K., Ohashi, H., Mizuno, S., Ogata, T., Kure, S. *et al.* (2012) Prevalence and clinical features of Costello syndrome and cardio-facio-cutaneous syndrome in Japan: findings from a nationwide epidemiological survey. *Am. J. Med. Genet. A*, **158A**, 1083–1094.
7. Malumbres, M. and Barbacid, M. (2003) RAS oncogenes: the first 30 years. *Nat. Rev. Cancer*, **3**, 459–465.
8. Aoki, Y., Niihori, T., Banjo, T., Okamoto, N., Mizuno, S., Kurosawa, K., Ogata, T., Takada, F., Yano, M., Ando, T. *et al.* (2013) Gain-of-function mutations in RIT1 cause Noonan syndrome, a RAS/MAPK pathway syndrome. *Am. J. Hum. Genet.*, **93**, 173–180.
9. Aoki, Y., Niihori, T., Narumi, Y., Kure, S. and Matsubara, Y. (2008) The RAS/MAPK syndromes: novel roles of the RAS pathway in human genetic disorders. *Hum. Mutat.*, **29**, 992–1006.
10. Tidyman, W.E. and Rauen, K.A. (2009) The RASopathies: developmental syndromes of Ras/MAPK pathway dysregulation. *Curr. Opin. Genet. Dev.*, **19**, 230–236.
11. Davies, H., Bignell, G.R., Cox, C., Stephens, P., Edkins, S., Clegg, S., Teague, J., Woffendin, H., Garnett, M.J., Bottomley, W. *et al.* (2002) Mutations of the BRAF gene in human cancer. *Nature*, **417**, 949–954.
12. Andreadi, C., Cheung, L.K., Giblett, S., Patel, B., Jin, H., Mercer, K., Kamata, T., Lee, P., Williams, A., McMahon, M. *et al.* (2012) The intermediate-activity (L597 V) BRAF mutant acts as an epistatic modifier of oncogenic RAS by enhancing signaling through the RAF/MEK/ERK pathway. *Genes Dev.*, **26**, 1945–1958.
13. Sarkozy, A., Carta, C., Moretti, S., Zampino, G., Digilio, M.C., Pantaleoni, F., Scioletti, A.P., Esposito, G., Cordeddu, V., Lepri, F. *et al.* (2009) Germline BRAF mutations in Noonan, LEOPARD, and cardiofaciocutaneous syndromes: molecular diversity and associated phenotypic spectrum. *Hum. Mutat.*, **30**, 695–702.
14. Storm, S.M., Cleveland, J.L. and Rapp, U.R. (1990) Expression of raf family proto-oncogenes in normal mouse tissues. *Oncogene*, **5**, 345–351.
15. Wojnowski, L., Stancato, L.F., Larner, A.C., Rapp, U.R. and Zimmer, A. (2000) Overlapping and specific functions of Braf and Craf-1 proto-oncogenes during mouse embryogenesis. *Mech. Dev.*, **91**, 97–104.
16. Wojnowski, L., Zimmer, A.M., Beck, T.W., Hahn, H., Bernal, R., Rapp, U.R. and Zimmer, A. (1997) Endothelial apoptosis in Braf-deficient mice. *Nat. Genet.*, **16**, 293–297.
17. Mercer, K., Giblett, S., Green, S., Lloyd, D., DaRocha Dias, S., Plumb, M., Marais, R. and Pritchard, C. (2005) Expression of endogenous oncogenic V600E B-raf induces proliferation and developmental defects in mice and transformation of primary fibroblasts. *Cancer Res.*, **65**, 11493–11500.
18. Urosevic, J., Sauzeau, V., Soto-Montenegro, M.L., Reig, S., Desco, M., Wright, E.M., Canamero, M., Mulero, F., Ortega, S., Bustelo, X.R. *et al.* (2011) Constitutive activation of B-Raf in the mouse germ line provides a model for human cardio-facio-cutaneous syndrome. *Proc. Natl. Acad. Sci. USA*, **108**, 5015–5020.
19. Watanabe, Y., Miyagawa-Tomita, S., Vincent, S.D., Kelly, R.G., Moon, A.M. and Buckingham, M.E. (2010) Role of mesodermal FGF8 and FGF10 overlaps in the development of the arterial pole of the heart and pharyngeal arch arteries. *Circ. Res.*, **106**, 495–503.
20. Packer, L.M., East, P., Reis-Filho, J.S. and Marais, R. (2009) Identification of direct transcriptional targets of (V600E)BRAF/MEK signalling in melanoma. *Pigment Cell Melanoma Res.*, **22**, 785–798.
21. Deng, Y., Atri, D., Eichmann, A. and Simons, M. (2013) Endothelial ERK signaling controls lymphatic fate specification. *J. Clin. Invest.*, **123**, 1202–1215.
22. Bekker, M.N., Twisk, J.W., Bartelings, M.M., Gittenberger-de Groot, A.C. and van Vugt, J.M. (2006) Temporal relationship between increased nuchal translucency and enlarged jugular lymphatic sac. *Obstet. Gynecol.*, **108**, 846–853.
23. Makinen, T., Norrmen, C. and Petrova, T.V. (2007) Molecular mechanisms of lymphatic vascular development. *Cell Mol. Life Sci.*, **64**, 1915–1929.
24. Chen, P.C., Wakimoto, H., Conner, D., Araki, T., Yuan, T., Roberts, A., Seidman, C., Bronson, R., Neel, B., Seidman, J.G. *et al.* (2010) Activation of multiple signaling pathways causes developmental defects in mice with a Noonan syndrome-associated Sos1 mutation. *J. Clin. Invest.*, **120**, 4353–4365.
25. Kruidenier, L., Chung, C.W., Cheng, Z., Liddle, J., Che, K., Joberty, G., Bantscheff, M., Bountra, C., Bridges, A., Diallo, H. *et al.* (2012) A selective jumonji H3K27 demethylase inhibitor modulates the proinflammatory macrophage response. *Nature*, **488**, 404–408.

26. Lee, S., Lee, J.W. and Lee, S.K. (2012) UTX, a histone H3-lysine 27 demethylase, acts as a critical switch to activate the cardiac developmental program. *Dev. Cell*, **22**, 25–37.
27. Welstead, G.G., Creyghton, M.P., Bilodeau, S., Cheng, A.W., Markoulaki, S., Young, R.A. and Jaenisch, R. (2012) X-linked H3K27me3 demethylase Utx is required for embryonic development in a sex-specific manner. *Proc. Natl. Acad. Sci. USA*, **109**, 13004–13009.
28. Zaidi, S., Choi, M., Wakimoto, H., Ma, L., Jiang, J., Overton, J.D., Romano-Adesman, A., Bjornson, R.D., Breitbart, R.E., Brown, K.K. *et al.* (2013) De novo mutations in histone-modifying genes in congenital heart disease. *Nature*, **498**, 220–223.
29. Hamada, S., Suzuki, T., Mino, K., Koseki, K., Oehme, F., Flamme, I., Ozasa, H., Itoh, Y., Ogasawara, D., Komaarashi, H. *et al.* (2010) Design, synthesis, enzyme-inhibitory activity, and effect on human cancer cells of a novel series of jumonji domain-containing protein 2 histone demethylase inhibitors. *J. Med. Chem.*, **53**, 5629–5638.
30. Croonen, E.A., Nillesen, W.M., Stuurman, K.E., Oudesluijs, G., van de Laar, I.M., Martens, L., Ockeloen, C., Mathijssen, I.B., Schepens, M., Ruiterkamp-Versteeg, M. *et al.* (2013) Prenatal diagnostic testing of the Noonan syndrome genes in fetuses with abnormal ultrasound findings. *Eur. J. Hum. Genet.*, **21**, 936–942.
31. Nisbet, D.L., Griffin, D.R. and Chitty, L.S. (1999) Prenatal features of Noonan syndrome. *Prenat. Diagn.*, **19**, 642–647.
32. de Mooij, Y.M., van den Akker, N.M., Bekker, M.N., Bartelings, M.M., van Vugt, J.M. and Gittenberger-de Groot, A.C. (2011) Aberrant lymphatic development in euploid fetuses with increased nuchal translucency including Noonan syndrome. *Prenat. Diagn.*, **31**, 159–166.
33. Romano, A.A., Allanson, J.E., Dahlgren, J., Gelb, B.D., Hall, B., Pierpont, M.E., Roberts, A.E., Robinson, W., Takemoto, C.M. and Noonan, J.A. (2010) Noonan syndrome: clinical features, diagnosis, and management guidelines. *Pediatrics*, **126**, 746–759.
34. Marin, T.M., Keith, K., Davies, B., Conner, D.A., Guha, P., Kalaitzidis, D., Wu, X., Lauriol, J., Wang, B., Bauer, M. *et al.* (2011) Rapamycin reverses hypertrophic cardiomyopathy in a mouse model of LEOPARD syndrome-associated PTPN11 mutation. *J. Clin. Invest.*, **121**, 1026–1043.
35. Wu, X., Simpson, J., Hong, J.H., Kim, K.H., Thavarajah, N.K., Backx, P.H., Neel, B.G. and Araki, T. (2011) MEK-ERK pathway modulation ameliorates disease phenotypes in a mouse model of Noonan syndrome associated with the Raf1(L613 V) mutation. *J. Clin. Invest.*, **121**, 1009–1025.
36. Schuhmacher, A.J., Guerra, C., Sauzeau, V., Canamero, M., Bustelo, X.R. and Barbacid, M. (2008) A mouse model for Costello syndrome reveals an Ang II-mediated hypertensive condition. *J. Clin. Invest.*, **118**, 2169–2179.
37. Kooistra, S.M. and Helin, K. (2012) Molecular mechanisms and potential functions of histone demethylases. *Nat. Rev. Mol. Cell. Biol.*, **13**, 297–311.
38. He, A., Ma, Q., Cao, J., von Gise, A., Zhou, P., Xie, H., Zhang, B., Hsing, M., Christodoulou, D.C., Cahan, P. *et al.* (2012) Polycomb repressive complex 2 regulates normal development of the mouse heart. *Circ. Res.*, **110**, 406–415.
39. Lederer, D., Grisart, B., Digilio, M.C., Benoit, V., Crespin, M., Ghariani, S.C., Maystadt, I., Dallapiccola, B. and Verellen-Dumoulin, C. (2012) Deletion of KDM6A, a histone demethylase interacting with MLL2, in three patients with Kabuki syndrome. *Am. J. Hum. Genet.*, **90**, 119–124.
40. Inagawa, M., Nakajima, K., Makino, T., Ogawa, S., Kojima, M., Ito, S., Ikenishi, A., Hayashi, T., Schwartz, R.J., Nakamura, K. *et al.* (2013) Histone H3 lysine 9 methyltransferases, G9a and GLP are essential for cardiac morphogenesis. *Mech. Dev.*, **130**, 519–531.
41. Kretzschmar, M., Doody, J., Timokhina, I. and Massague, J. (1999) A mechanism of repression of TGFbeta/ Smad signaling by oncogenic Ras. *Genes Dev.*, **13**, 804–816.
42. Agger, K., Cloos, P.A., Rudkjaer, L., Williams, K., Andersen, G., Christensen, J. and Helin, K. (2009) The H3K27me3 demethylase JMJD3 contributes to the activation of the INK4A-ARF locus in response to oncogene- and stress-induced senescence. *Genes Dev.*, **23**, 1171–1176.
43. Fujii, S., Tokita, K., Wada, N., Ito, K., Yamauchi, C., Ito, Y. and Ochiai, A. (2011) MEK-ERK pathway regulates EZH2 overexpression in association with aggressive breast cancer subtypes. *Oncogene*, **30**, 4118–4128.
44. Krenz, M., Gulick, J., Osinska, H.E., Colbert, M.C., Molkentin, J.D. and Robbins, J. (2008) Role of ERK1/2 signaling in congenital valve malformations in Noonan syndrome. *Proc. Natl. Acad. Sci. USA*, **105**, 18930–18935.
45. Wan, P.T., Garnett, M.J., Roe, S.M., Lee, S., Niculescu-Duvaz, D., Good, V.M., Jones, C.M., Marshall, C.J., Springer, C.J., Barford, D. *et al.* (2004) Mechanism of activation of the RAF-ERK signaling pathway by oncogenic mutations of B-RAF. *Cell*, **116**, 855–867.
46. Pierpont, E.I., Pierpont, M.E., Mendelsohn, N.J., Roberts, A.E., Tworog-Dube, E., Rauen, K.A. and Seidenberg, M.S. (2010) Effects of germline mutations in the Ras/MAPK signaling pathway on adaptive behavior: cardiofaciocutaneous syndrome and Noonan syndrome. *Am. J. Med. Genet. A*, **152A**, 591–600.
47. Stevenson, D.A., Schwarz, E.L., Carey, J.C., Viskochil, D.H., Hanson, H., Bauer, S., Weng, H.Y., Greene, T., Reinker, K., Swensen, J. *et al.* (2011) Bone resorption in syndromes of the Ras/MAPK pathway. *Clin. Genet.*, **80**, 566–573.
48. Armour, C.M. and Allanson, J.E. (2008) Further delineation of cardio-facio-cutaneous syndrome: clinical features of 38 individuals with proven mutations. *J. Med. Genet.*, **45**, 249–254.
49. Matsumura, H., Hasuwa, H., Inoue, N., Ikawa, M. and Okabe, M. (2004) Lineage-specific cell disruption in living mice by Cre-mediated expression of diphtheria toxin A chain. *Biochem. Biophys. Res. Commun.*, **321**, 275–279.
50. Niwa, H., Yamamura, K. and Miyazaki, J. (1991) Efficient selection for high-expression transfectants with a novel eukaryotic vector. *Gene*, **108**, 193–199.

Ann Hematol (2014) 93:1515–1522
DOI 10.1007/s00277-014-2090-4

ORIGINAL ARTICLE

Identification of acquired mutations by whole-genome sequencing in GATA-2 deficiency evolving into myelodysplasia and acute leukemia

Tohru Fujiwara · Noriko Fukuhara · Ryo Funayama · Naoki Nariai · Mayumi Kamata · Takeshi Nagashima · Kaname Kojima · Yasushi Onishi · Yoji Sasahara · Kenichi Ishizawa · Masao Nagasaki · Keiko Nakayama · Hideo Harigae

Received: 27 February 2014 / Accepted: 13 April 2014 / Published online: 30 April 2014

Abstract Heterozygous *GATA-2* germline mutations are associated with overlapping clinical manifestations termed GATA-2 deficiency, characterized by immunodeficiency and predisposition to myelodysplastic syndrome (MDS) and acute myeloid leukemia (AML). However, there is considerable clinical heterogeneity among patients, and the molecular basis for the evolution of immunodeficiency into MDS/AML remains unknown. Thus, we conducted whole-genome sequencing on a patient with a germline GATA-2 heterozygous mutation (c. 988 C > T; p. R330X), who had a history suggestive of immunodeficiency and evolved into MDS/AML. Analysis was conducted with DNA samples from leukocytes for immunodeficiency, bone marrow mononuclear cells for MDS and bone marrow-derived mesenchymal stem cells. Whereas we did not identify a candidate genomic deletion that may contribute to the evolution into MDS, a total of 280 MDS-specific nonsynonymous single nucleotide variants were identified. By narrowing down with the single nucleotide polymorphism database, the functional missense database, and NCBI information, we finally identified three candidate mutations for *EZH2*, *HECW2* and *GATA-1*, which may contribute to the evolution of the disease.

Keywords GATA-2 · GATA-2 deficiency · MonoMAC · Myelodysplastic syndrome · Whole-genome sequencing · EZH2 · GATA-1

Electronic supplementary material The online version of this article (doi:10.1007/s00277-014-2090-4) contains supplementary material, which is available to authorized users.

T. Fujiwara · N. Fukuhara · M. Kamata · Y. Onishi · K. Ishizawa · H. Harigae (✉)
Department of Hematology and Rheumatology, Tohoku University Graduate School, 2-1 Seiryo-cho, Aoba-ku, Sendai 980-8575, Japan
e-mail: harigae@med.tohoku.ac.jp

T. Fujiwara · H. Harigae
Molecular Hematology/Oncology, Tohoku University Graduate School, Sendai, Japan

R. Funayama · T. Nagashima · K. Nakayama
Department of Cell Proliferation, United Center for Advanced Research and Translational Medicine, Tohoku University Graduate School, Sendai, Japan

N. Nariai · K. Kojima · M. Nagasaki
Department of Integrative Genomics, Tohoku Medical Megabank Organization, Tohoku University, Sendai, Japan

Y. Sasahara
Department of Pediatrics, Tohoku University Graduate School, Sendai, Japan

K. Ishizawa
Clinical Research, Innovation and Education Center, Tohoku University Hospital, Sendai, Japan

Introduction

GATA-2 is a zinc finger transcription factor that plays crucial roles in hematopoiesis, as well as vascular, lymphatic, and neural development [1]. Recently, heterozygous *GATA-2* germline mutations, both inherited and de novo, were reported to cause three overlapping clinical entities, characterized by a predisposition to myelodysplastic syndrome (MDS) and acute myeloid leukemia (AML): (1) familial MDS/AML, (2) Emberger syndrome and (3) an immunodeficiency termed monocytopenia characterized by mycobacterium avium complex (MonoMAC)/dendritic cell, monocyte, B- and NK-lymphoid deficiency (DCML) [2–4]. All these conditions are generally named "GATA-2 deficiency" syndrome.

Nearly half of the individuals presenting with GATA-2 mutations will eventually develop MDS/AML, associated with fibrosis and megakaryocyte dysplasia. In contrast, many patients gradually develop DCML before MDS/AML, initially detected as mild chronic neutropenia, monocytopenia and/or NK deficiency [2–4]. Therefore, there is considerable clinical heterogeneity among patients with GATA-2 deficiency, although all these conditions predominantly affect the hematologic and immune systems. In addition, the rate of evolution of the disease into MDS/AML appears to be rapid, with varying MDS and AML phenotypes and variable cytogenetic abnormalities [5, 6]. Therefore, secondary genetic events may explain the clinical heterogeneity among cases of GATA-2 deficiency. In this regard, the most commonly associated cytogenetic finding is monosomy 7 and additional acquired mutations, such as those in *ASXL1* [6]. However, the molecular basis for the evolution of GATA-2 deficiency into MDS/AML has not been elucidated, which affects our ability of early detection and treatment of the disease.

Whole-genome sequencing has several advantages over candidate gene sequencing. It provides a comprehensive and nonbiased approach to mutation detection. More importantly, whole-genome paired-end sequencing is able to detect structural variants (SV; e.g., deletions, amplifications, inversions and translocations). Therefore, to investigate the genetic changes associated with the evolution of GATA-2 deficiency into MDS/AML, we performed whole-genome sequencing of MDS sample, which was compared with matched samples from nail, leukocyte at immunodeficiency, and bone marrow-derived mesenchymal stem cells (BM-MSCs).

Patient and methods

Study design and clinical samples

All clinical samples were obtained from a single patient referred to our department for pancytopenia and emergence of myeloblasts in the peripheral blood. They included nails, peripheral leukocytes at immunodeficiency (MonoMAC), and bone marrow mononuclear cells for MDS (MDS). The patient signed an informed consent before sample collection, and all ethical considerations were followed according to the Declaration of Helsinki. This study was approved by the ethical committee of the Tohoku University Graduate School of Medicine.

Cell culture

Cells were grown in a humidified incubator at 37 °C with 5 % carbon dioxide. Human K562 erythroleukemia cell lines were maintained in Roswell Park Memorial Institute (RPMI-1640) medium containing 10 % fetal bovine serum (Biowest) and 1 % penicillin–streptomycin (Sigma). PLAT-GP Packaging Cell Lines (Cell Biolabs) was maintained in Dulbecco's modified Eagle medium (DMEM) containing 10 % fetal bovine serum (Biowest) and 1 % penicillin–streptomycin (Sigma).

Gene transfer and vectors

GATA-2 mRNA was cloned into pBABE-puro vector (Addgene Plasmid 1764) [7], and a single mutation was introduced with QuikChange Site-Directed Mutagenesis Kit (Agilent). The retroviral vector encoding human GATA-2 and the env (envelope glycoprotein) gene from the vesicular stomatitis virus (VSV-G) were co-transfected into PLAT-GP cells with FuGene HD (Promega). Seventy-two hours after transfection, the viral supernatant was used for infection. After spin infection into CD34-positive cells at 3,400 rpm for 2 h, the cells were cultured containing 1 μg/mL Puromycin (Sigma) for the selection of the transduced cells.

Quantitative ChIP analysis

Real-time-PCR-based quantitative chromatin immunoprecipitation (ChIP) analysis was conducted essentially as described [8]. Cells were crosslinked with 1 % formaldehyde for 10 min at room temperature. The nuclei lysate was sonicated to reduce DNA length using Sonifier (Branson). The protein-DNA complexes were immunoprecipitated by specific antibody and Protein A Sepharose (Sigma). Immunoprecipitated DNA fragments were quantified by real-time PCR to amplify regions of 75–150 bp overlapping with the appropriate motif. Product was measured by SYBR Green fluorescence in 20-μL reactions, and the amount of product was determined relative to a standard curve generated from titration of input chromatin. Analysis of post-amplification dissociation curves showed that primer pairs generated single products.

Primers

Primers used in the study were listed in Table 1.

Western blot analysis

Whole cell extracts were prepared by boiling cells for 10 min in SDS sample buffer [25 mM Tris (pH 6.8), 2 % β-mercaptoethanol, 3 % SDS, 0.1 % bromophenol blue, 5 % glycerol] at 1×10^7 cells/mL. Extracts from 1 to 2×10^5 cells were resolved by SDS-PAGE and transferred to Hybond-P (GE Healthcare). The proteins were measured by semi-quantitatively with ECL-Plus (GE Healthcare) and CL-X Posure™ Film (Thermo Scientific).

Table 1 Oligonucleotide primers

Designation	Forward and reverse sequences(5′-3′)
Primers used for GATA-2 sequencing	
GATA-2 exon 2	GTTTTGAGCCTTGGGCTTT
	CAATTTTTCAGCAGCTCGATT
GATA-2 exon 3	GGAGTCGTGATCTCAATGTCTG
	ATCTGCTGGGGGCTATTAGAG
GATA-2 exon 4	ACTCCCTCCCGAGAACTTG
	CGTCTGCATTTGAAGGAGTTT
GATA-2 exon 5	GAGATTTAGCCCTCCTTGACTG
	AGCACAAAGCGCAGAGGT
GATA-2 exon 6	GAAGGTCGGGCACAATTC
	ACAGGTGCCATGTGTCCA
Primers used for validation sequencing	
EZH2	CATCAAAAGTAACACATGGAAACC
	GCTGCTTTAAAACATAATTCCACA
HECW2	GTCCATATCCTACCTCCAGTAGC
	GACAGCTCCTGCAATGAGAGT
GATA-1	TAGACCTTGGGCAGCTCCT
	CCTTGGTAGAGATGGGCAGTA
Primers used for quantitative ChIP	
GATA-2 −2.4 kb	GTGGAGCTCTAGGGTACCATTT
	TGAGGACACCTCATTAGAGCAG
GATA-2 −3.5 kb	GTCCGGGGTAATTTTTCATCT
	GCAGATAACGACTGGCTATTCA
GATA-2 −4.6 kb	GAGATGAGCTAATCCCGCCGTA
	AAGGCTGTATTTTTCCAGGCT
NECDIN promoter	GAAGAGCTCCTGGACGCAGA
	TGCAAAGTTAGGGTCGCTCAG

Antibodies

Antibodies to GATA-2 (H-116) and Actin (I-19) were obtained from Santa Cruz Biotechnology. Control rabbit IgG was obtained from Abcam. Phycoerythrin (PE)-labeled human CD29, PE-labeled human CD34, fluorescein isothiocyanate (FITC)-labeled mouse/human CD44, FITC-labeled human CD45, FITC-labeled human CD90 antibodies were purchased from BD Biosciences.

The anti-GATA-2 antibody (H-116) recognizes amino acid residues 120–235 of human GATA-2.

Flow cytometry (FACS)

The cells collected from culture were washed twice with phosphate-buffered saline (PBS; Sigma). The cells were then incubated with PE- and FITC-labeled antibodies, washed twice with PBS, and analyzed using FACSAria II (Beckton, Dickinson). The collected data were processed with FlowJo software (http://www.flowjo.com/).

Establishment of BM-MSCs

To establish BM-MSCs, bone marrow mononuclear cells from the patient were cultured in DMEM (Life Technologies) supplemented with 20 % fetal bovine serum (Life Technologies), 10 ng/mL basic fibroblast growth factor (PeproTech), 10 mM HEPES (Life Technologies), and 100 μg/mL penicillin/streptomycin, as previously described [9]. To induce differentiation into osteroblasts and adipocytes, the hMSC Mesenchymal Stem Cell Differentiation Medium (Lonza) for osteogenic and adipogenic, respectively, was used. Osteogenic cell layers were positive for Alkaline Phosphatase staining, and typical adipocytes contained oil drops that were stained with Oil Red O.

Genome analysis

To identify MDS-specific genome alterations, whole-genome sequencing was conducted on MonoMAC, MDS and BM-MSCs (Fig. 1). Genomic DNA was extracted with the DNeasy Blood & Tissue Kit (QIAGEN) or ISOHAIR (NIPPON GENE). For whole-genome sequencing, the DNA samples were amplified with the REPLI-g Midi Kit (QIAGEN). Sequencing libraries were prepared from 1 μg of the amplified DNA according to the TruSeq DNA Sample Prep Guide (Illumina). The libraries were sequenced on an Illumina HiSeq 2000 with HiSeq control software (HCS) version 1.5 and Real-Time Analysis (RTA) software version 1.13. After sequencing, reads were mapped to the human reference genome (GRCh37/hg19) with decoy sequences (hs37d5) using BWA [10] with the default options. Then, variant calling was conducted using the GATK Unified Genotyper [11].

Sanger sequence-based validation analysis was conducted with all samples, including the nail sample, using an ABI 3730xl DNA analyzer and the ABI BigDye Terminator Cycle Sequencing Kit (Applied Biosystems). The validation analyses were conducted based on the DNA samples without amplification.

Results and discussion

Case report

In September 2010, a 35-year-old man was referred to our department due to pancytopenia and emergence of myeloblasts in the peripheral blood. Peripheral blood count revealed a white blood cell count of 1.2×10^9/L, with 79 % neutrophils, 16 % lymphocytes, 1 % eosinophils, 1 % atypical lymphocytes, and 3 % myeloblasts. The hemoglobin level was 9.8 g/dl, and the platelet count was 27×10^9/L. Bone marrow analysis indicated a total nucleated cell count of 2.2×10^{10}/L, with dysplastic morphological changes in all lineages. The bone

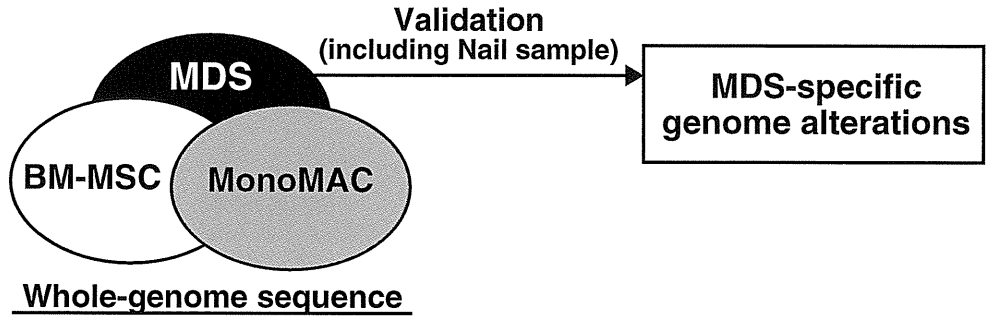

Fig. 1 Study design. Whole-genome sequencing conducted with MonoMAC, MDS and BM-MSCs samples to identify MDS-specific genome alterations. Sanger sequence-based validation analysis was conducted on all samples, including a nail sample

marrow contained 11 % leukemic blasts, all positive for CD7, CD13, CD33, CD34, and HLA-DR. Cytogenetic analysis indicated the presence of trisomy 8. The patient was diagnosed with MDS, classified into the refractory anemia with excess blasts (RAEB-2), and had "Very high" risk according to the criteria of revised international prognostic index (IPSS-R) [12]. In January 2011, the case rapidly developed into AML, and received hematopoietic stem cell transplantation from a matched unrelated donor with reduced intensity conditioning regimen.

Since the age of 16 years, he had been treated for nontuberculous mycobacterial infection, cryptococcal meningitis and recurrent cutaneous human papilloma virus infection. For this reason, he was initially diagnosed with primary immunodeficiency. There was no family history of increased susceptibility to infection, or onset of MDS/AML. Based on our clinical findings and the family history, we suspected that the patient might have sporadic MonoMAC syndrome.

Identification of a germline GATA-2 mutation

Sanger sequencing for *GATA-2* cDNA revealed a 988 C > T heterozygous mutation (Fig. 2a). We confirmed that the mutation was germline because it involved the nail sample (Fig. 2a). This mutation resulted in the generation of a premature stop codon at Arg330, located in the N-terminal zinc finger domain (Fig. 2a). As GATA-2 DNA binding activity is mediated through the C-terminal zinc finger domain [1], the mutated GATA-2 is predicted to be defective in DNA binding. To test the hypothesis, we overexpressed wild-type or mutated (R330X) GATA-2 in K562 cells (Fig. 2b). Quantitative ChIP analysis was conducted with anti-GATA-2 antibody at endogenous loci (GATA-2 −4.6, −3.5 and −2.4 kb), which were selected from GATA-2 ChIP-seq analysis based on K562 cells [8]. As shown in Fig. 2c, GATA-2 chromatin occupancy was obviously increased by overexpression of wild-type GATA-2. However, although the antibody could recognize GATA-2 330X (Fig. 2b), the levels of GATA-2 chromatin occupancy in GATA-2 R330X-overexpressing K562 cells were similar to the control cells. Thus, we consider that the heterozygous GATA-2 R330X mutation is a loss-of-function mutation.

Generation and characterization of BM-MSCs

We established BM-MSCs from BM mononuclear cells from the patient, and used for the reference control for whole-genome analysis. Immunophenotypic analysis confirmed that the BM-MSCs expressed typical markers, i.e., CD29, CD44, CD90, and CD105, but not CD14, CD34, and CD45 (Supplementary Fig. 1a) [13]. Furthermore, the established BM-MSCs had the capacity to differentiate into adipocytes and osteoblasts (Supplementary Fig. 1b). Sanger sequencing also confirmed that the cells harbored the identical *GATA-2* mutation (Fig. 2a).

Whole-genome sequencing identified mutations in EZH2, HECW2, and GATA-1

To elucidate the secondary genetic changes associated with the evolution to MDS/AML, we performed whole-genome sequencing with DNA samples from nail, MonoMAC, MDS, and BM-MSCs (Fig. 1). However, the data from the nail sample were excluded from the analysis due to a low mapping rate of the sequence on the human genome.

First, we focused on the MDS-specific genome deletion. GATA-2 plays a crucial role in the proliferation of hematopoietic stem cells (HSCs) [1, 14]. Thus, it is possible that *GATA-2* haploinsufficient HSCs could have a reduced proliferative activity. Therefore, secondary deletions involving oncogenic genes, such as a tumor suppressor gene, may promote the evolution to MDS/AML. In support of this hypothesis, a recent study revealed that a heterozygous 3-kb deletion, removing exons 7–9 of *TP53* gene, was associated with the onset of therapy-related AML through whole-genome sequencing [15]. To identify the MDS-specific gene deletion, we used several SV callers, including BreakDancer, Pindel, and CNVnator, as described previously [16]. However, we failed to identify the candidate genomic deletion that may contribute to the evolution into MDS.

Our next strategy was to sort out the point mutations, using the GATK Unified Genotyper [11]. They were observed in the MDS sample, but not in MonoMAC or BM-MSCs. A total of 280 MDS-specific nonsynonymous single nucleotide variants (nsSNVs) were identified, which were subsequently narrowed

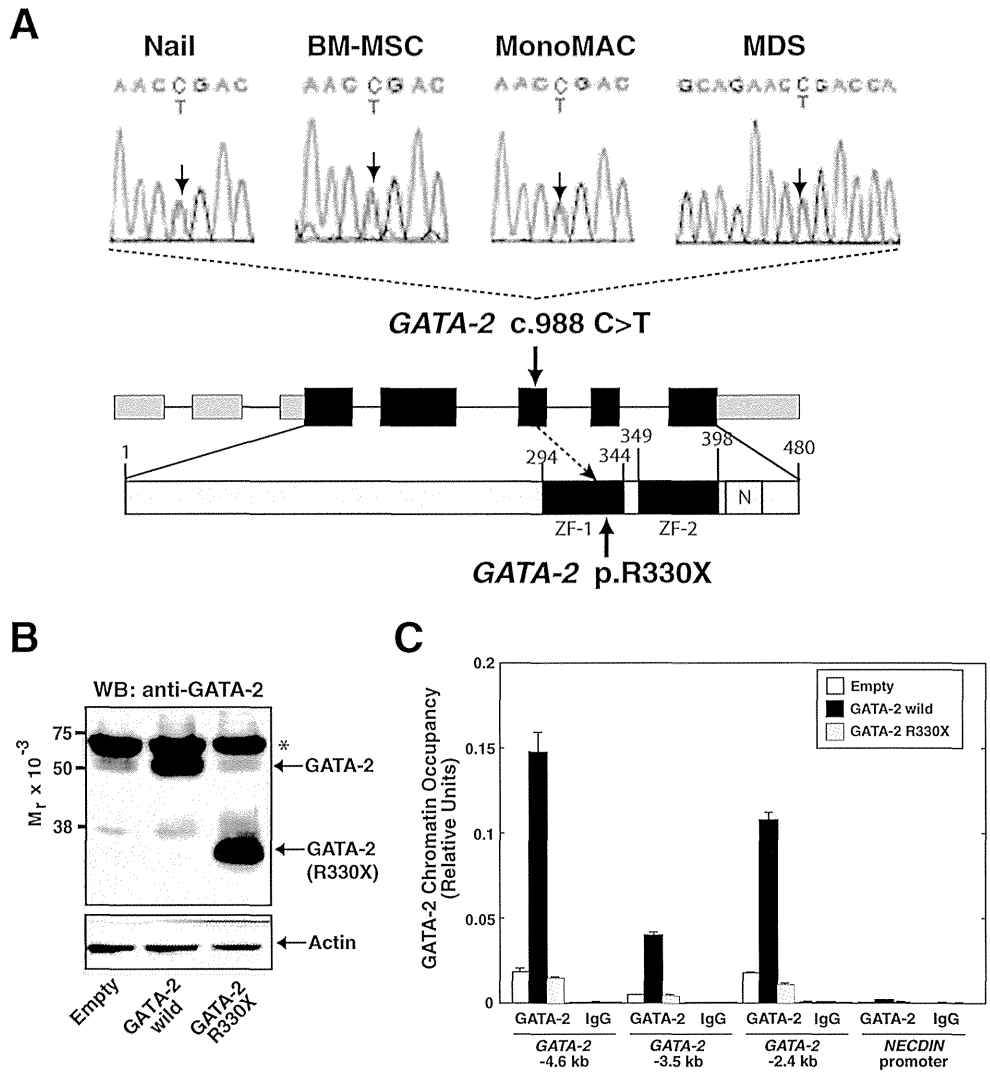

Fig. 2 Identification of a germline heterozygous GATA-2 mutation. **a** Heterozygous germline GATA-2 mutation was confirmed with the nail, BM-MSC, MonoMAC and MDS samples: *GATA-2* c. 988 C > T, p. R330X. ZF, zinc finger. Numbering relative to adenine in the ATG start codon of *GATA-2* (GenBank NM_001145661.1) and the first methionine (GenBank NP_116027.2) [3]. **b** Western blot analysis to detect wild-type and mutated GATA-2 in K562 cells. Actin was used as a loading control. GATA-2 R330X was detected by the anti-GATA-2 antibody (H-116), as it recognizes amino acid residues 120–235 of human GATA-2. Asterisk, cross-reactive band. **c** Quantitative ChIP analysis to examine GATA-2 occupancy in wild-type and mutated GATA-2-overexpressing K562 cells (n=3, mean±SD). *NECDIN* promoter was included as a negative control

down based on the single nucleotide polymorphism (SNP) database, the functional missense database and NCBI information (http://www.ncbi.nlm.nih.gov; Table 2). Finally, we identified three candidate mutations, namely EZH2 (Enhancer of zeste homolog 2, Drosophila), HECW2 (HECT, C2 and WW domain containing E3 ubiquitin protein ligase 2), and GATA-1 (GATA-binding protein 1; Table 2, Fig. 3). Sanger sequence-based validation analysis confirmed that all three mutations were observed only in the MDS sample (Fig. 3). As expected, the peak height of the mutated signal was lower than that of the wild-type signal, presumably reflecting the frequency of leukemic blasts (11 %).

Table 2 Point mutations identified in MDS sample

Functional missense database								
Name	Chr.	Depth	SIFT	PolyPhen2	LJB_PhyloP	LJB MutationTaster	LJB_LRT	AA Change
EZH2	7	49	0.06	0.926	0.9839	0.9995	1.0	E210K
HECW2	2	61	0.06	0.002	0.03258	0.005	0.0318	V701M
GATA-1	X	21	0	0.944	0.99824	0.9999	1.0	R293Q

Three mutations were not identified in SNP database (dbSNP130 and 1000G_ALL)

Chr chromosome, *SIFT* sorting intolerant from tolerant, *PolyPhen2* polymorphism phenotyping v2, *LJB_PhyloP* pathogenicity score from dbNSFP, *LJB_MutationTaster* pathogenicity probability score from dbNSFP, *LJB_LRT* pathogenicity probability score from dbNSFP, *AA* amino acid.

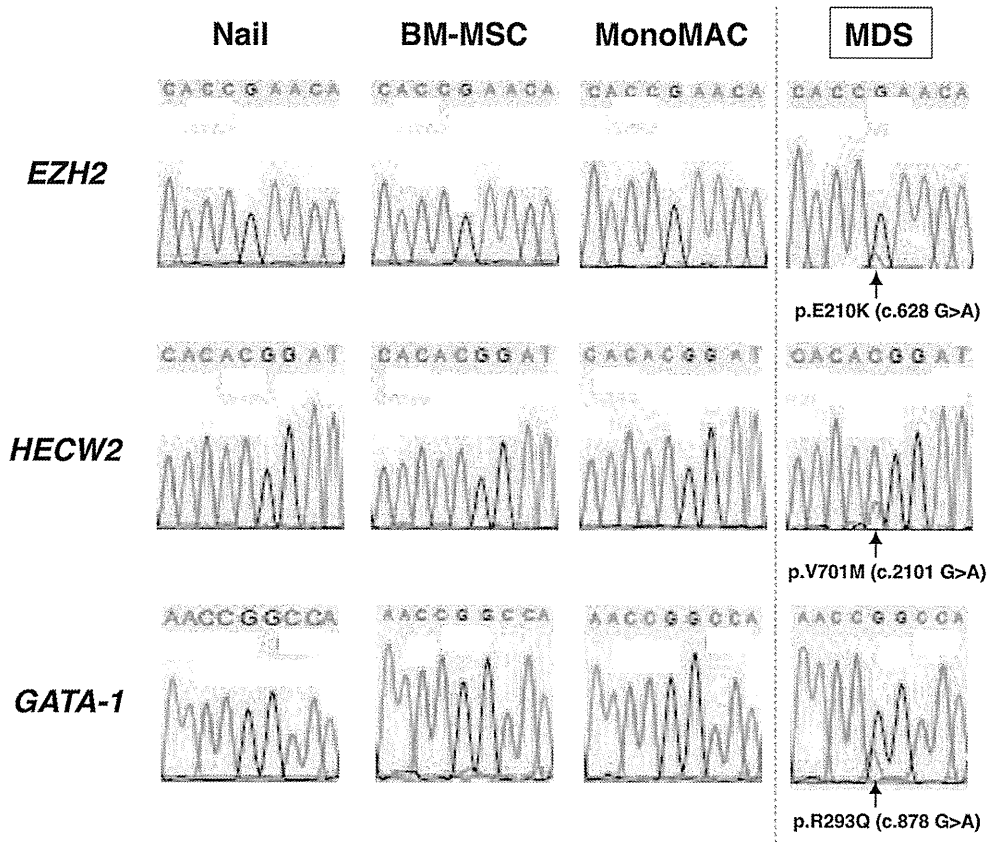

Fig. 3 Validation analysis for MDS-specific point mutations. Validation analysis of the MDS-specific point mutations. Sanger sequence conducted to validate point mutations identified by whole-genome sequencing. For the *HECW2* mutation, the nucleotide substitution was described as opposite strand (G > A to C > T)

EZH2 is a member of the Polycomb group, which is involved in the maintenance of the transcriptional repressive state of genes by trimethylation of histone H3 at lysine 27 [17]. It is well established that EZH2 loss-of-function mutations are frequently identified in MDS [18]. Amino acid position at 210 (Glu) is located at SWI3-ADA2-N-CoR-TFIIIB (SANT) domain that has been shown to interact both with histone tails and with other proteins [19]. Whereas gain-of-function mutations of EZH2 have also been attributable to pathogenesis of lymphoma, the mutations were observed at the C-terminal catalytic SET domain (Y641 and Y677) [20]. Thus, we assume that the EZH2 E210K mutation could be loss-of-function mutation. HECW2 is predicted to be ubiquitin ligase that degrades ATR (ataxia-telangiectasia-mutated-and-Rad3-related) kinase [21]. However, its role in hematopoiesis is unknown. Finally, GATA-1 is a member of the GATA transcription factors promoting erythrocyte, megakaryocyte, mast cell, and eosinophil development [1]. Amino acid position at 293 (Arg) is located in the C-terminal zinc finger domain, which is important for the recognition of the (A/T)GATA(A/G) motif, and to confer its transcriptional activity [1]. Noticeably, a recent report suggests that defective GATA-1 function results in the dyserythropoiesis, which is characteristic of MDS [22]. Based on the functional missense database, the mutations of both E210K on EZH2 and R293Q on GATA-1 may have significant effect on their endogenous functions (Table 2). In support of the hypothesis, mutation frequencies for EZH2 (38.8 %) and GATA-1 (38.1 %) were higher than HECW2 (24.6 %; Fig. 4). Thus, at least two secondary mutations in EZH2 and GATA-1 may have contributed to the early stage of clonal evolution into MDS in the

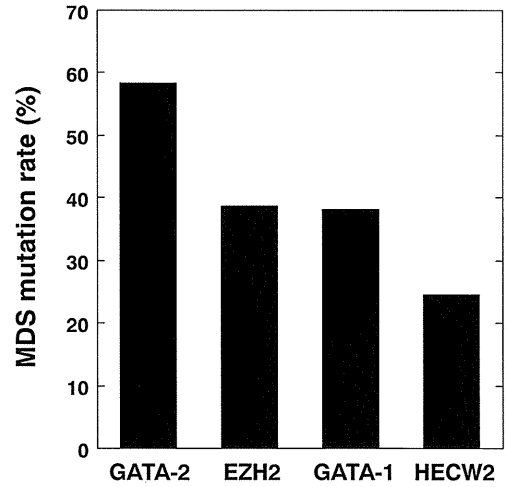

Fig. 4 Quantification of the mutation load for EZH2, GATA-1 and HECW2. Percentage of the mutated reads per the total number of reads (both wild-type and mutated) in MDS sample was calculated for GATA-2 (c. 988 C > T), EZH2 (c. 628 G > A), GATA-1 (c. 878 G > A) and HECW2 (c. 2101 G > A)

present case. Future investigations are needed to determine the possible involvement of HECW2 mutation.

In conclusion, we conducted whole-genome sequencing with samples from a patient with germline GATA-2 mutation evolving immunodeficiency and MDS/AML. The new mutations we identified in *EZH2*, *HECW2* and *GATA-1* appear to be important secondary events leading to the development of MDS/AML of this patient.

Acknowledgements We thank Drs. Mamoru Takahashi, Riu Yamashita, Kengo Kinoshita, and Kazuhiko Igarashi (Tohoku University) for their helpful discussions. We acknowledge the members of the Biomedical Research Core of Tohoku University School of Medicine and Biomedical Research Unit of Tohoku University Hospital for their support. Drs. Fujiwara and Harigae have received a research grant from Chugai Pharmaceutical Co., Ltd.

Conflict of interest All authors declared no conflict of interest.

References

1. Bresnick EH, Lee HY, Fujiwara T, Johnson KD, Keles S (2010) GATA switches as developmental drivers. J Biol Chem 285:31087–31093. doi:10.1074/jbc.R110.159079
2. Dickinson RE, Griffin H, Bigley V, Reynard LN, Hussain R, Haniffa M, Lakey JH, Rahman T, Wang XN, McGovern N, Pagan S, Cookson S, McDonald D, Chua I, Wallis J, Cant A, Wright M, Keavney B, Chinnery PF, Loughlin J, Hambleton S, Santibanez-Koref M, Collin M (2011) Exome sequencing identifies GATA-2 mutation as the cause of dendritic cell, monocyte, B and NK lymphoid deficiency. Blood 118:2656–2658. doi:10.1182/blood-2011-06-360313
3. Hsu AP, Sampaio EP, Khan J, Calvo KR, Lemieux JE, Patel SY, Frucht DM, Vinh DC, Auth RD, Freeman AF, Olivier KN, Uzel G, Zerbe CS, Spalding C, Pittaluga S, Raffeld M, Kuhns DB, Ding L, Paulson ML, Marciano BE, Gea-Banacloche JC, Orange JS, Cuellar-Rodriguez J, Hickstein DD, Holland SM (2011) Mutations in GATA2 are associated with the autosomal dominant and sporadic monocytopenia and mycobacterial infection (MonoMAC) syndrome. Blood 118:2653–2655. doi:10.1182/blood-2011-05-356352
4. Ostergaard P, Simpson MA, Connell FC, Steward CG, Brice G, Woollard WJ, Dafou D, Kilo T, Smithson S, Lunt P, Murday VA, Hodgson S, Keenan R, Pilz DT, Martinez-Corral I, Makinen T, Mortimer PS, Jeffery S, Trembath RC, Mansour S (2011) Mutations in GATA2 cause primary lymphedema associated with a predisposition to acute myeloid leukemia (Emberger syndrome). Nat Genet 43:929–931. doi:10.1038/ng.923
5. Hahn CN, Chong CE, Carmichael CL, Wilkins EJ, Brautigan PJ, Li XC, Babic M, Lin M, Carmagnac A, Lee YK, Kok CH, Gagliardi L, Friend KL, Ekert PG, Butcher CM, Brown AL, Lewis ID, To LB, Timms AE, Storek J, Moore S, Altree M, Escher R, Bardy PG, Suthers GK, D'Andrea RJ, Horwitz MS, Scott HS (2011) Heritable GATA2 mutations associated with familial myelodysplastic syndrome and acute myeloid leukemia. Nat Genet 43:1012–1017. doi:10.1038/ng.913
6. Bödör C, Renneville A, Smith M, Charazac A, Iqbal S, Etancelin P, Cavenagh J, Barnett MJ, Kramarzová K, Krishnan B, Matolcsy A, Preudhomme C, Fitzgibbon J, Owen C (2012) Germ-line GATA2 p.THR354MET mutation in familial myelodysplastic syndrome with acquired monosomy 7 and ASXL1 mutation demonstrating rapid onset and poor survival. Haematologica 97:890–894. doi:10.3324/haematol.2011.054361
7. Morgenstern JP, Land H (1990) Advanced mammalian gene transfer: high titre retroviral vectors with multiple drug selection markers and a complementary helper-free packaging cell line. Nucleic Acids Res 18:3587–3596
8. Fujiwara T, O'Geen H, Keles S, Blahnik K, Kang YA, Harigae H, Choi K, Farnham PJ, Bresnick EH (2009) Discovering hematopoietic mechanisms through genome-wide analysis of GATA factor chromatin occupancy. Mol Cell 36:667–681. doi:10.1016/j.molcel.2009.11.001
9. Solchaga LA, Penick K, Porter JD, Goldberg VM, Caplan AI, Welter JF (2005) FGF-2 enhances the mitotic and chondrogenic potentials of human adult bone marrow-derived mesenchymal stem cells. J Cell Physiol 203:398–409
10. Li H, Durbin R (2009) Fast and accurate short read alignment with Burrows-Wheeler transform. Bioinformatics 25:1754–1760. doi:10.1093/bioinformatics/btp324
11. McKenna A, Hanna M, Banks E, Sivachenko A, Cibulskis K, Kernytsky A, Garimella K, Altshuler D, Gabriel S, Daly M, DePristo MA (2010) The Genome Analysis Toolkit: a MapReduce framework for analyzing next-generation DNA sequencing data. Genome Res 20:1297–1303. doi:10.1101/gr.107524.110
12. Greenberg PL, Tuechler H, Schanz J, Sanz G, Garcia-Manero G, Solé F, Bennett JM, Bowen D, Fenaux P, Dreyfus F, Kantarjian H, Kuendgen A, Levis A, Malcovati L, Cazzola M, Cermak J, Fonatsch C, Le Beau MM, Slovak ML, Krieger O, Luebbert M, Maciejewski J, Magalhaes SM, Miyazaki Y, Pfeilstöcker M, Sekeres M, Sperr WR, Stauder R, Tauro S, Valent P, Vallespi T, van de Loosdrecht AA, Germing U, Haase D (2012) Revised international prognostic scoring system for myelodysplastic syndromes. Blood 120:2454–2465. doi:10.1182/blood-2012-03-420489
13. Pittenger MF, Mackay AM, Beck SC, Jaiswal RK, Douglas R, Mosca JD, Moorman MA, Simonetti DW, Craig S, Marshak DR (1999) Multilineage potential of adult human mesenchymal stem cells. Science 284:143–147
14. Tsai FY, Orkin SH (1997) Transcription factor GATA-2 is required for proliferation/survival of early hematopoietic cells and mast cell formation, but not for erythroid and myeloid terminal differentiation. Blood 89:3636–3643
15. Link DC, Schuettpelz LG, Shen D, Wang J, Walter MJ, Kulkarni S, Payton JE, Ivanovich J, Goodfellow PJ, Le Beau M, Koboldt DC, Dooling DJ, Fulton RS, Bender RH, Fulton LL, Delehaunty KD, Fronick CC, Appelbaum EL, Schmidt H, Abbott R, O'Laughlin M, Chen K, McLellan MD, Varghese N, Nagarajan R, Heath S, Graubert TA, Ding L, Ley TJ, Zambetti GP, Wilson RK, Mardis ER (2011) Identification of a novel TP53 cancer susceptibility mutation through whole-genome sequencing of a patient with therapy-related AML. JAMA 305:1568–1576. doi:10.1001/jama.2011.473
16. Suzuki S, Yasuda T, Shiraishi Y, Miyano S, Nagasaki M (2011) ClipCrop: a tool for detecting structural variations with single-base resolution using soft-clipping information. BMC Bioinformatics 12(Suppl 14):S7. doi:10.1186/1471-2105-12-S14-S7
17. Müller J, Hart CM, Francis NJ, Vargas ML, Sengupta A, Wild B, Miller EL, O'Connor MB, Kingston RE, Simon JA (2002) Histone methyltransferase activity of a Drosophila Polycomb group repressor complex. Cell 111:197–208
18. Cazzola M, Della Porta MG, Malcovati L (2013) The genetic basis of myelodysplasia and its clinical relevance. Blood 122:4021–4034. doi:10.1182/blood-2013-09-381665

19. Yu J, Li Y, Ishizuka T, Guenther MG, Lazar MA (2003) A SANT motif in the SMRT corepressor interprets the histone code and promotes histone deacetylation. EMBO J 22:3403–3410
20. McCabe MT, Ott HM, Ganji G, Korenchuk S, Thompson C, Van Aller GS, Liu Y, Graves AP, Della Pietra A 3rd, Diaz E, LaFrance LV, Mellinger M, Duquenne C, Tian X, Kruger RG, McHugh CF, Brandt M, Miller WH, Dhanak D, Verma SK, Tummino PJ, Creasy CL (2012) EZH2 inhibition as a therapeutic strategy for lymphoma with EZH2-activating mutations. Nature 492:108–112. doi:10.1038/nature11606
21. Muralikrishna B, Chaturvedi P, Sinha K, Parnaik VK (2012) Lamin misexpression upregulates three distinct ubiquitin ligase systems that degrade ATR kinase in HeLa cells. Mol Cell Biochem 365:323–332. doi:10.1007/s11010-012-1272-4
22. Frisan E, Vandekerckhove J, de Thonel A, Pierre-Eugène C, Sternberg A, Arlet JB, Floquet C, Gyan E, Kosmider O, Dreyfus F, Gabet AS, Courtois G, Vyas P, Ribeil JA, Zermati Y, Lacombe C, Mayeux P, Solary E, Garrido C, Hermine O, Fontenay M (2012) Defective nuclear localization of Hsp70 is associated with dyserythropoiesis and GATA-1 cleavage in myelodysplastic syndromes. Blood 119:1532–1542. doi:10.1182/blood-2011-03-343475

PLOS | ONE

HCV Infection Enhances Th17 Commitment, Which Could Affect the Pathogenesis of Autoimmune Diseases

Yasuteru Kondo[1]*, Masashi Ninomiya[1], Osamu Kimura[1], Keigo Machida[2], Ryo Funayama[3], Takeshi Nagashima[3], Koju Kobayashi[1], Eiji Kakazu[1], Takanobu Kato[4], Keiko Nakayama[3], Michael M. C. Lai[2,5], Tooru Shimosegawa[1]

1 *Division of Gastroenterology, Tohoku University Graduate School of Medicine, Sendai City, Miyagi, Japan,* **2** *Department of Microbiology and Immunology, Keck School of Medicine, University of Southern California, Los Angeles, California, United States of America,* **3** Division of Cell Proliferation, Tohoku University Graduate School of Medicine, Sendai City, Miyagi, Japan, **4** Department of Virology II, National Institute of Infectious Diseases, Shinjuku, Tokyo, Japan, **5** China Medical University, Taichung, Taiwan

Abstract

Background: Various kinds of autoimmune diseases have been reported to have a significant relationship with persistent hepatitis c virus (HCV) infection and Th17 cells. Previously, our group reported that the existence of HCV in T lymphocytes could affect the development of $CD4^+$ helper T cells and their proliferation, in addition to the induction of immunoglobulin hyper-mutation.

Methods: Therefore, we analyzed the relationship between persistent infection of HCV and the mechanism of Th17 cell induction *ex vivo* and *in vitro*.

Results: The prevalence of autoimmune-related diseases in chronic hepatitis c patients (CH-C) was significantly higher than in other types of chronic hepatitis (hepatitis B and NASH). A significantly higher frequency of IL6 and TGF-β double-high patients was detected in CH-C than in other liver diseases. Moreover, these double-high patients had significantly higher positivity of anti-nuclear antibody, cryoglobulinemia, and lymphotropic HCV and higher amounts of IL1-β, IL21, IL23. In addition to the previously reported lymphotropic SB-HCV strain, we found a novel, genotype 1b lymphotropic HCV (Ly-HCV), by deep sequencing analysis. Lymphotropic-HCV replication could be detected in the lymphoid cells with various kinds of cytokine-conditions including IL1β, IL23, IL6 and TGF-β in vitro. Infection by HCV could significantly enhance the development of Th17 cells. The HCV protein responsible for inducing the Th17 cells was HCV-Core protein, which could enhance the STAT-3 signaling and up-regulate the expression of RORγt as a Th17 master gene.

Conclusion: Infection by lymphotropic HCV might enhance the Th17 development and contribute to understanding the pathogenesis of autoimmune-related diseases.

Citation: Kondo Y, Ninomiya M, Kimura O, Machida K, Funayama R, et al. (2014) HCV Infection Enhances Th17 Commitment, Which Could Affect the Pathogenesis of Autoimmune Diseases. PLoS ONE 9(6): e98521. doi:10.1371/journal.pone.0098521

Editor: Stephen J. Polyak, University of Washington, United States of America

Received February 20, 2014; **Accepted** May 2, 2014; **Published** June 6, 2014

Funding: This work was supported in part by Grant-in Aid from the Ministry of Education, Culture, Sport, Science, and Technology of Japan (Y.K. #21790642, #23790761 and #25460970), Grant from the Japan Society of Hepatology (Y.K), the National Institute on Alcohol Abuse and Alcoholism (K.M. #R01 AA018857) and the American Cancer Society (K.M. #RSG-12-177-01). The funders had no role in study design, data collection and analysis, decision to publish, or preparation of the manuscript.

Competing Interests: The authors have declared that no competing interests exist.

* E-mail: yasuteru@ebony.plala.or.jp

Introduction

Cellular and humoral immune responses to HCV play an important role in the pathogenesis of chronic hepatitis, HCC and B-lymphocyte proliferative disorders including mixed cryoglobulinemia, a disorder characterized by the oligoclonal proliferation of B cells [1–5]. B cell activation and/or dis-regulation could originate as a result of HCV binding to CD81 tetraspanin molecule or as a consequence of its ability to replicate in B lymphocytes[6]. It has been reported that HCV could infect B lymphocytes[7–9]. We previously reported that HCV-replication in B lymphocytes could induce immunoglobulin hypermutation and reduce the affinity and neutralizing activities of antibodies against HCV envelope protein[5]. On the other hand, the hypermutation of immunoglobulin might induce autoantibodies that contribute to the immunopathogenesis of autoimmune diseases, since various kinds of autoimmune diseases were reported to have a significant relationship with persistent HCV infection [10–12].

Previously, our group reported that the existence of HCV in T lymphocytes could affect the development and proliferation of type 1 T helper (Th1) cells[3,4,13]. Other groups have also reported the existence of HCV in T lymphocytes[14,15]. HCV replication in T lymphocytes could suppress Interferon-γ (IFN-γ)/signal transducers and activators of transcription factor 1 (STAT-1) signaling that might affect signal transducers and activators of transcription factor 3 (STAT-3) signaling[4,13].

It has been reported that a subset of type 17 T helper (Th17) cells might be involved in various kinds of autoimmune diseases[16–19]. The orphan nuclear receptor RORγt (RORγt) is the key transcription factor that induces the transcription of the genes encoding Interleukin (IL)-17 in naïve $CD4^+$ T helper cells[20]. Moreover, the activation of STAT-3 signaling could contribute to the induction of Th17 development[21–23]. Previously, Machida et al. reported that HCV replication in B lymphocytes could enhance the production of IL-6 from B lymphocyte[24]. In addition to TGF-β1, the existence of IL-6 could enhance the development of Th17 cells. IL17A-producing T lymphocytes have been recently shown to comprise a distinct lineage of pro-inflammatory T helper cells, termed Th17 cells, that are major contributors to autoimmune disease[20]. IL17A stimulates the secretion of a wide range of proinflammatory chemokines and cytokines. As its receptor is widely expressed, various kinds of immune cells as well as other cell types can respond to it[25]. Recently, we reported that the frequency of Th17 cells was remarkably high in a difficult-to-treat case of pyoderma gangrenosum-like lesion in a patient with lymphotropic HCV infection[26].

In this study, we clarified the relationship between Th17 cells and the biological significance of lymphotropic HCV.

Material and Methods

Study design and Patients

Two hundred-fifty patients with HCV persistent infection who were treated in Tohoku University Hospital were enrolled in this study. None of the patients had liver disease due to other causes, such as alcohol, drug, or congestive heart failure. Permission for the study was obtained from the Ethics Committee at Tohoku University Graduate School of Medicine (permission no. 2006–194) following ethical guidelines of the 1975 Declaration of Helsinki. Written informed consent was obtained from all the participants enrolled in this study. Participants were monitored for 6 months and peripheral blood samples were obtained from selected patients. We collected the peripheral blood before the treatment (treatment naïve). The concurrent diseases were diagnosed by specialized physicians belonging to the department of hematology and rheumatology. Patients were evaluated for serum levels of HCV-RNA, blood chemistry and hematology.

Quantification of IL1β, IL6, Transforming growth factor 1 (TGF-β1) and IL17A, IL21, IL23 in the serum

The amounts of IL1β, IL6, TGF-β1, IL17A, IL21 and IL23 were quantified using IL1β, IL6, TGF-β, IL17A, IL21 and IL23 enzyme-linked immunosorbent assay (ELISA) kits (eBioscience). The serum samples from patients were collected at sampling points and stored at −20°C. The ELISA procedure was performed according to the manufacturer's protocol.

Isolation of peripheral blood mononuclear cells (PBMCs), $CD4^+$ cells, $CD19^+$ cells and $CD45RA^+$ naïve $CD4^+$ cells

PBMCs were isolated from fresh heparinized blood by means of Ficoll-Paque (Amersham Bioscience) density gradient centrifugation. $CD4^+$ T cells and $CD19^+$ B cells were positively isolated by dynabeads (Dynal) to carry out the analysis of strand-specific HCV RNA detection. Naïve $CD4^+$ cells were isolated by the MACS beads system (Miltenyi Biotec).

Strand-specific intracellular HCV RNA detection

Strand-specific intracellular HCV RNA was detected using a recently established procedure that combined previously published methods [27,28] with minor modifications [4,13]. Positive- and negative-strand-specific HCV RNAs were detected by a nested polymerase chain reaction (PCR) method. Semi-quantification was achieved by serial fourfold dilutions (in 10 μg/ml of *Escherichia coli* tRNA) of an initial amount of 200 ng of total RNA. The relative titer was expressed as the highest dilution giving a visible band of the appropriate size on a 2% agarose gel stained by ethidium bromide. For the internal control, semi-quantification of β-actin mRNA was performed using the same RNA extracts. To rule out false, random, and self-priming, extracted HCV RNA was run in every RT–PCR test without the addition of an upstream HCV primer.

The deep-sequencing analysis of Ly-HCV

Serum samples and PBMCs were collected from a patient with para-aortic lymph node enlargement with chronic HCV infection. Serum samples were stored at −20°C until testing. Total RNA was extracted from 800 μl of serum and 1.0×10^7 of PBMC using Trizol LS (Invitrogen). Each library was prepared using TruSeq RNA sample preparation kits v2 (Illumina). Libraries were clonally amplified on the flow cell and sequenced on an Illumina HiSeq 2000 (HiSeq Control Software 1.5, Illumina) with a 101-mer paired end sequence. Image analysis and base calling were performed using Real Time Analysis (RTA) 1.13. In the first mapping analysis, sequence reads not of human origin were aligned with 27675 reference virus sequences registered at the Hepatitis virus database server (HVDB) (http://s2as02.genes.nig.ac.jp/index.html) and the National Center for Biotechnology Information (NCBI) (http://www.ncbi.nlm.nih.gov/) using bwa (0.5.9-r26) and allowing mismatches of within 10 nucleotide bases. Based on the highest homology to the reference virus genome in the first mapping analysis, the tentative consensus HCV full genome sequence was created. The second mapping analysis was conducted using the tentative consensus HCV full genome sequence and bwa, allowing mismatches of within 5 nucleotide bases. The result of the analysis was displayed using Integrative Genomics Viewer (IGV; 2,0,17). Sequence analysis was performed using Genetyx-Mac ver.12. A phylogenetic tree was constructed by the unweighted pair group method with the arithmetic mean. The reliability of the phylogenetic results was assessed using 100 bootstrap replicate.

Inoculation of lymphotropic HCV strains in various kinds of lymphoid cell lines and human primary lymphocyte with stimulation

We used two different lymphotropic HCV strains. One was the SB-HCV strain that was previously reported by Sung et al[29]. The other one was Ly-HCV that was identified in this study by our group. The almost full-length sequence (95.9% coverage) of Ly-HCV was determined using a deep-sequence Hi-Seq 2000 system (illumina) (Fig S1A and B). These two-lymphotropic HCV strains were used for the experiments of HCV infection into lymphoid cells. Previously, we reported Raji, Molt-4 and primary human lymphoid cells were susceptible to the SB-HCV strain. In addition to these cells, we used miR122-transduced RIG-1/MDA-knockdown Raji cells provided by Machida K et al, since this cell line was most susceptible to SB-HCV replication (ongoing project, data not shown). These lymphotropic HCV strains were inoculated at day 0. SB cell culture supernatant and diluted serum from the patient with Ly-HCV, which contained 2×10^5 copies/ml of HCV-

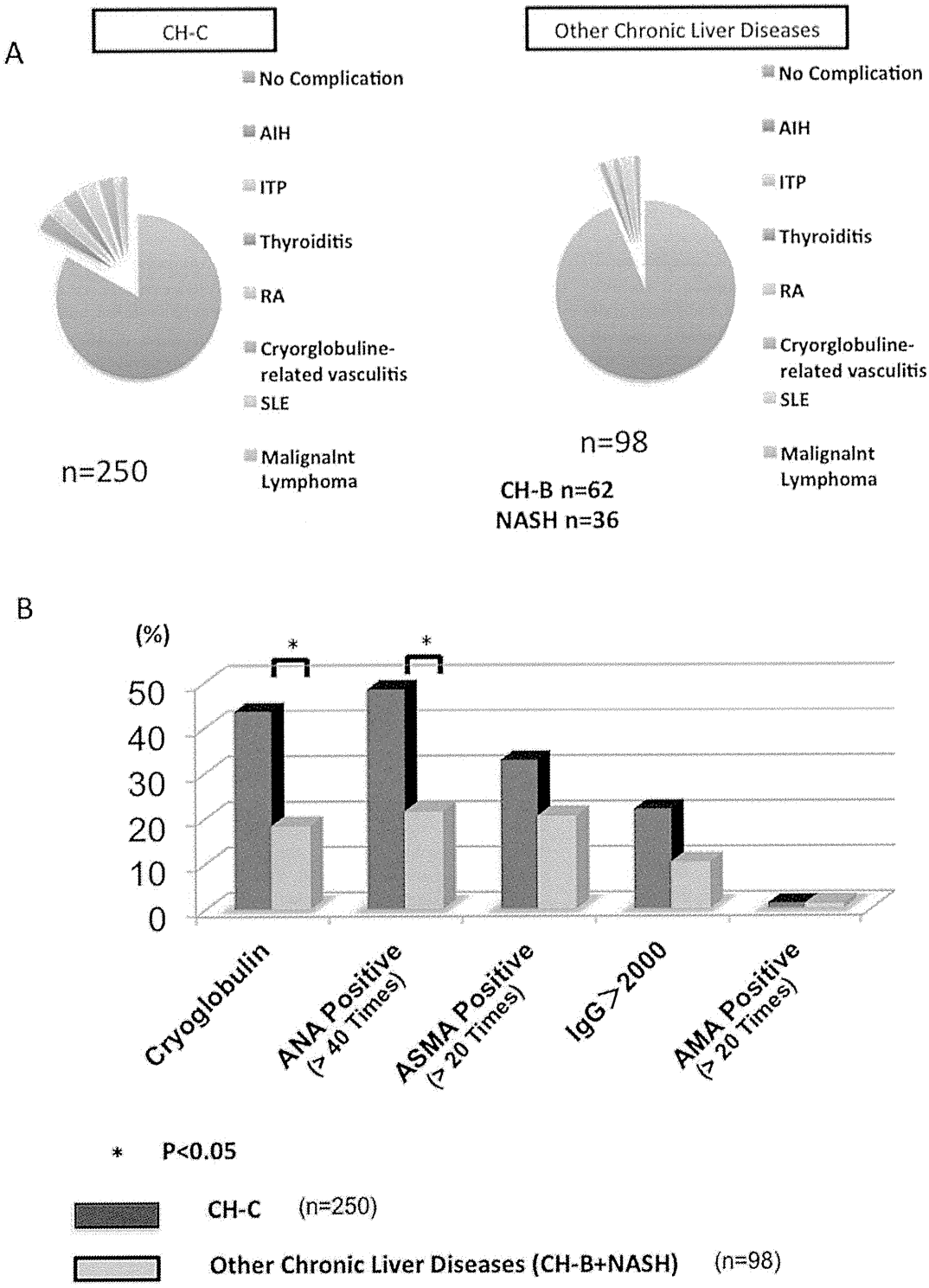

Figure 1. The relation between CH-C and the phenotype of autoimmune- diseases. The prevalence of these diseases in CH-C (n = 250) was significantly higher than in other chronic liver diseases (n = 98) (p = 0.0011) (A). The prevalence of these diseases and the positive rate of cryoglobulin, ANA (>40 times), ASMA (>20 times) and AMA (>20 times), and the amount of IgG (>2000mg/dl) are shown (B).
doi:10.1371/journal.pone.0098521.g001

RNA, were used for the infection of several kinds of human primary lymphoid cells (1×10^5 cells). A control infection with UV-irradiated HCV was included in every experiment. The supernatant of Huh-7 cells transfected with JFH-1 strains at 10 days post-transfection was used for several control experiments. The HCV-1T strain obtained from a CH-C patient without extrahepatic diseases and lymphoproliferative diseases was also used for several control experiments.

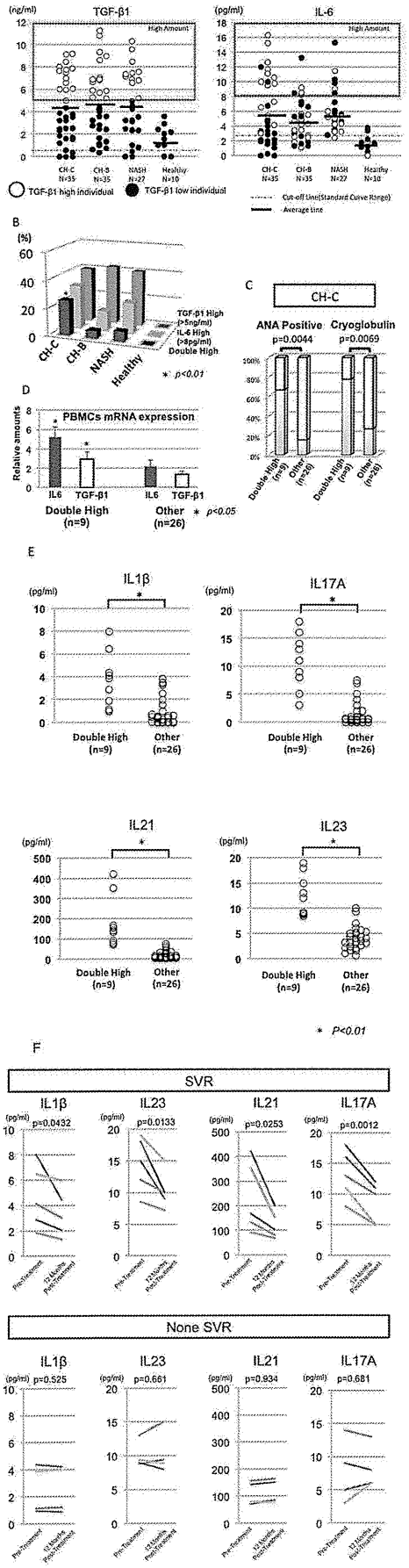

Figure 2. The cytokine conditions affecting the positivity of ANA and Cryoglobulin, and Th17 development. A comparison of the amounts of IL6 and TGF-β among the CH-C, CH-B, NASH and healthy subjects is shown (A). The bar indicates the mean cytokine amounts. The frequency of TGF-β1 high, IL6 high, and TGF-β1 and IL6 double high patients among the 4 groups (CH-C, CH-B, NASH, and healthy subjects) is shown (B). The positive rate of ANA and Cryoglobulin in the double high CH-C patients (n = 9) and the other CH-C patients (n = 26) is shown(C). The IL6 and TGF-β1 mRNA expression of PBMCs in the double-high patients (n = 9) and other patients (n = 26) is shown in the bar graphs (D). The amounts of IL1β, IL17A, IL21 and IL23 in the serum were compared between double high CH-C patients (n = 9) and the other CH-C patients (n = 26) (E). The comparisons of serum cytokines before and after the Peg-interferon/Ribavirin treatment are shown (F). Serum samples were collected at just before the treatment and twelve month after the end of treatment. SVR indicates sustained virological treatment (n = 5).
doi:10.1371/journal.pone.0098521.g002

The analysis of IL17-secreting CD4$^+$ T cells

Naïve CD4$^+$ cells were negatively isolated by using a naïve CD4$^+$ T cells isolation kit II (Miltenyi Biotec). Isolated naïve CD4$^+$ cells were exposed to SB-HCV, Ly-HCV, UV-irradiated-SB-HCV, UV-irradiated-Ly-HCV or Mock. Then, CD3$^+$CD28$^+$ coated beads and various kinds of cytokines were added to the culture medium to analyze the Th17 commitment and development (Table S1). The cytokine conditions for Th17 commitment and development included IL-1β (10 ng/ml), and IL23 (1 ng/ml), which are important for the Th17 development in human, because the differentiation of Th17 cells is very difficult without these cytokines when using human PBMCs[30]. The cells were harvested at 7 days post-inoculation and IL17A-secreting cells were analyzed by MACS cytokine secretion assay (Miltenyi Biotec).

Transwell co-culture system

The trans-membrane with 0.4 um pore size was used for the analysis of soluble factor-inducing Th17 cells, especially IL6 and TGF-β1. The upper chamber included PBMCs (2×10^6 cells/ml) of CH-C patients (Ly-HCV or HCV-1T). The lower chamber included naïve CD4$^+$ cells (2×10^5 cells/ml) of a healthy individual and CD3CD28 coated beads with or without IL6 (40 ng/ml)(abcam) and TGF-β1 (40 ng/ml)(abcam) neutralizing antibodies. After five days incubation, the total RNA was isolated from cells of the lower chamber. The expression levels of RORγt were analyzed by real time PCR.

Construction of Lenti-virus expressing HCV-Core antigen

HCV core cDNA cloned in pcDNA3 was kindly provided by Dr. K. Takeuchi [31]. The full length HCV core cDNA was cloned into lentiviral vector, pCSII-EF plasmid, to create the pCSII-EF-HCV core[32]. The pCSII-EF-HCV core or control pCSII-EF-IRES-GFP plasmid was transfected into HEK293T cells together with two packaging plasmids, pCAG-HIVgp and pCMV-VSV-G/RSV-Rev (provided by the RIKEN Bio-resource Center), using the calcium phosphate method. The supernatants containing the recombinant lenti-virus were used for the infection of human primary lymphocyte.

Transfection of HCV individual protein expression plasmids

Various expression plasmids were constructed by inserting HCV-core, E1, E2, NS3, NS4B, NS5A and NS5B cDNA of genotype 1a behind the cytomegalovirus immediate-early promoter in pCDNA3.1 (Invitrogen). Primary CD4$^+$ cells were transfect-

Table 1. The frequency of Strand specific-HCV-RNA positive CD4+ T cells and CD19+ B cells.

		Negative-st-positive		Positive-st-positive	
		%(n: positive/total)		%(n: postive/total)	
	Double High (n=9)	33.3 (3/9)		44.4 (4/9)	
CD4+ T cell			p=0.0166		p=0.033
	Other (n=26)	3.8 (1/26)		11.5 (3/26)	
	Double High (n=9)	44.4 (4/9)		66.6 (6/9)	
CD19+ B cell			p=0.0027		p=0.0003
	Other (n=26)	3.8 (1/26)		7.6 (2/26)	

St-specific HCV-RNA were detected by nested PCR with rTth polymerase.
Double high indicates that the amount of IL6 and TGF-β are high.
doi:10.1371/journal.pone.0098521.t001

ed using 4D-Nucleofector II (Amaxa, Gaithersburg, Washington DC, USA) with a human T cell nucleofector kit (Amaxa), and various plasmids were purified using the EndFree plasmid kit (QIAGEN, Valencia, CA, USA). Viable transfected cells were isolated by Ficoll-Paque centrifugation (Amersham Bioscience) at 24 hour post-transfection. The transfection and expression efficiencies were analyzed using intracellular staining of individual proteins of HCV and flow cytometry analysis.

Real-time PCR analysis

Cells were collected before the inoculation of lenti-virus and 10 days after the inoculation of lenti-virus. Total RNA was isolated using a column isolation kit (QIAGEN). After the isolation of RNA, one-step real-time PCR using a TaqMan Chemistry System was carried out. The ready-made set of primers and probe for the amplification of IL-6 (Hs00985639_m1), TGF-β1 (Hs00998133_m1), T-bet (Hs00203436_m1), GATA-3 (Hs00231122_m1), RORC (Hs01076112_m1) and glyceraldehyde-3-phosphate dehydrogenase (GAPDH) (Hs03929097_g1) were purchased from Applied Biosystems. The relative amount of target mRNA was obtained using a comparative threshold cycle (CT) method. The expression level of mRNAs of the non-stimulation sample of mock infected $CD4^+$ cells was represented as 1.0 and the relative amounts of target mRNA were calculated according to the manufacturer's protocol.

The analysis of STAT-1 and STAT-3 signaling

STAT-1 and STAT-3 signaling was analyzed by phospho-STAT-1 (Tyr701) and phosphor-STAT-3 (Tyr705) sandwich ELISA kit (Cell Signaling Technology). Briefly, naïve $CD4^+$ cells transfected with or without HCV-core expressing plasmid were incubated with IL6 and TGF-β1. The cells were harvested at various time points. Then, the cell lysates were used for the quantification of phosphor-STAT-1 and phosphor-STAT-3.

Statistical analysis

The data in Figure 1A, 1B, 2B and 2C were analyzed by χ^2 test. The data in Figure 2D and 2E were analyzed by independent Students t test. Figure 3A, 3C, 4A, 4B and 4C were analyzed by Mann-Whitney U test. All statistical analyses were carried out using JMP Pro version 9.

Accession Numbers

Accession number EntryID
AB779562 51027b2b6a8011fb860007e4.LyHCVserumSR
Accession number EntryID
AB779679 51029c6f6a8011fb8600093e.LyHCVpbmcSR

Results

Prevalence of autoimmune-related diseases in the CH-C patients

The prevalence of autoimmune-related disease in the CH-C patients was significantly higher than in the subjects with other chronic liver diseases in Tohoku University Hospital (p = 0.0011) (Fig.1A). In addition to the prevalence of autoimmune-related diseases, we analyzed the immunological laboratory tests including cryoglobulin, anti-nuclear antibody (ANA), anti-smooth muscle antibodies (ASMA), Immunoglobulin G (IgG), anti-mitochondrial antibody (AMA). The frequency of ANA positive or cryoglobulin positive patients in CH-C patients was significantly higher than in those with other chronic liver diseases ($p<0.05$) (Fig.1B).

The amount of IL6 and TGF-β1 in the peripheral blood of CH-C patients

The average amounts of IL6 and TGF-β1 were comparable among healthy subjects, CH-C, CH-B and NASH (IL6: 1.77, 5.83, 4.84 and 5.99 pg/ml), (TGF-β: 1.45, 4.18, 4.68 and 4.5 mg/ml), (average amount) (Fig. 2A). However, the frequency of patients with high amounts of IL6 (over 8 pg/ml) and TGF-β1 (over 5 ng/ml) (double-high) was significantly higher than in those with other chronic liver diseases ($p<0.05$)(Fig. 2B). The cut-off levels of high amount of IL6 (over 8 pg/ml) and TGF-β1 (over 5 ng/ml) were determined by the appearance of two clusters(high and low) in the CH-C samples. Interestingly, Most of the TGF-β1 high CH-C patients had high amounts of IL6 (Fig. 2B). Moreover, the amount of IL6 were significantly correlated with the amount of TGF-β1(data not shown). The serum amounts of IL6 and TGFβ1 were analyzed at 6 months after the sampling points. The serum amount of IL6 and TGF-β1 in the high amount of IL6 and TGF-β1 both (double-high) patients remained doubly high (data not shown). It has been reported that the combination of IL6 and TGF-β1 cytokines could induce Th17 cells[20]. Therefore, we compared the frequency of ANA-positive or cryoglobulin-positive patients between double-high patients and the other patients with HCV persistent infection. The frequency of ANA-positive or cryoglobulin-positive patients among the double-high patients was significantly higher than among the other CH-C patients ($p<0.01$)(Fig. 2C). The expression of IL-6 and TGF-β1-mRNA in PBMCs of double-high patients was significantly higher than in other CH-C patients ($p<0.05$)(Fig. 2D). Moreover, the serum amounts of IL1-β, IL17A, IL21 and IL23 in the double-high

Table 2. The frequency of different nucleotide bases between LyHCVserumSR and LyHCVpbmcSR.

Nucleo tide Position	LyHCVserumSR										LyHCVpbmcSR									
	Max base	No. of nucleotide	A (%)		C (%)		G (%)		T (%)		Max base	No. of nucleotide	A (%)		C (%)		G (%)		T (%)	
538	G	1835	482	(26.27)	3	(0.16)	1349	(73.51)	1	(0.05)	A	1	1	(100.0)	0	(0.00)	0	(0.00)	0	(0.00)
659	G	1821	484	(26.58)	1	(0.05)	1334	(73.26)	2	(0.11)	A	1	1	(100.0)	0	(0.00)	0	(0.00)	0	(0.00)
1,026	A	2041	1098	(53.80)	2	(0.10)	939	(46.01)	2	(0.10)	G	3	1	(33.33)	0	(0.00)	2	(66.67)	0	(0.00)
1,034	C	2120	4	(0.19)	1263	(59.58)	0	(0.00)	853	(40.24)	T	3	0	(0.00)	1	(33.33)	0	(0.00)	2	(66.67)
1,280	C	2050	2	(0.10)	1785	(87.07)	2	(0.10)	261	(12.73)	T	7	0	(0.00)	2	(28.57)	0	(0.00)	5	(71.43)
2,050	C	1595	11	(0.69)	930	(58.31)	652	(40.88)	2	(0.13)	G	4	0	(0.00)	1	(25.00)	3	(75.00)	0	(0.00)
2,105	T	1852	1	(0.05)	587	(31.70)	0	(0.00)	1264	(68.25)	C	6	0	(0.00)	4	(66.67)	0	(0.00)	2	(33.33)
2,114	A	1814	1261	(69.51)	525	(28.94)	22	(1.21)	6	(0.33)	C	7	3	(42.86)	4	(57.14)	0	(0.00)	0	(0.00)
2,136	T	1813	0	(0.00)	527	(29.07)	1	(0.06)	1285	(70.88)	C	7	0	(0.00)	4	(57.14)	0	(0.00)	3	(42.86)
2,159	T	1904	0	(0.00)	505	(26.52)	1	(0.05)	1398	(73.42)	C	7	0	(0.00)	4	(57.14)	0	(0.00)	3	(42.86)
2,234	C	2023	5	(0.25)	1128	(55.76)	3	(0.15)	887	(43.85)	T	9	0	(0.00)	3	(33.33)	0	(0.00)	6	(66.67)
2,249	C	2030	5	(0.25)	1471	(72.46)	0	(0.00)	554	(27.29)	T	8	0	(0.00)	3	(37.50)	0	(0.00)	5	(62.50)
2,717	G	1841	471	(25.58)	1	(0.05)	1365	(74.14)	4	(0.22)	A	3	2	(66.67)	0	(0.00)	1	(33.33)	0	(0.00)
3,878	T	2449	3	(0.12)	37	(1.51)	1	(0.04)	2408	(98.33)	C	3	0	(0.00)	2	(66.67)	0	(0.00)	1	(33.33)
4,043	C	1894	14	(0.74)	1836	(96.94)	0	(0.00)	44	(2.32)	T	3	0	(0.00)	1	(33.33)	0	(0.00)	2	(66.67)
4,473	C	2105	811	(38.53)	1292	(61.38)	1	(0.05)	1	(0.05)	A	5	4	(80.00)	1	(20.00)	0	(0.00)	0	(0.00)
4,661	C	2263	2	(0.09)	1301	(57.49)	1	(0.04)	959	(42.38)	T	6	0	(0.00)	0	(0.00)	0	(0.00)	6	(100.0)
5,087	G	2050	477	(23.27)	1	(0.05)	1572	(76.68)	0	(0.00)	A	5	3	(60.00)	0	(0.00)	2	(40.00)	0	(0.00)
5,114	G	1791	32	(1.79)	452	(25.24)	1306	(72.92)	1	(0.06)	C	3	0	(0.00)	2	(66.67)	1	(33.33)	0	(0.00)
5,117	A	1674	1262	(75.39)	1	(0.06)	411	(24.55)	0	(0.00)	G	3	1	(33.33)	0	(0.00)	2	(66.67)	0	(0.00)
5,156	G	1871	481	(25.71)	0	(0.00)	1389	(74.24)	0	(0.00)	A	3	2	(66.67)	0	(0.00)	1	(33.33)	0	(0.00)
5,462	C	2026	2	(0.10)	1452	(71.67)	3	(0.15)	569	(28.08)	T	11	0	(0.00)	3	(27.27)	0	(0.00)	8	(72.73)
5,535	T	2059	1	(0.05)	490	(23.80)	0	(0.00)	1568	(76.15)	C	9	0	(0.00)	5	(55.56)	0	(0.00)	4	(44.44)
5,799	G	2113	477	(22.57)	0	(0.00)	1634	(77.33)	1	(0.05)	A	3	2	(66.67)	0	(0.00)	1	(33.33)	0	(0.00)
5,804	C	2131	3	(0.14)	1613	(75.69)	3	(0.14)	511	(23.98)	T	3	0	(0.00)	1	(33.33)	0	(0.00)	2	(66.67)
5,807	T	2102	2	(0.10)	490	(23.31)	5	(0.24)	1604	(76.31)	C	3	0	(0.00)	2	(66.67)	0	(0.00)	1	(33.33)
5,831	T	2168	7	(0.32)	483	(22.28)	5	(0.23)	1672	(77.12)	C	3	0	(0.00)	2	(66.67)	0	(0.00)	1	(33.33)
5,834	T	2153	2	(0.09)	504	(23.41)	0	(0.00)	1647	(76.50)	C	3	0	(0.00)	3	(100.0)	0	(0.00)	0	(0.00)
5,837	C	2144	3	(0.14)	1674	(78.08)	2	(0.09)	465	(21.69)	T	3	0	(0.00)	1	(33.33)	0	(0.00)	2	(66.67)
5,882	T	2160	0	(0.00)	480	(22.22)	0	(0.00)	1680	(77.78)	C	3	0	(0.00)	2	(66.67)	0	(0.00)	1	(33.33)
5,883	C	2114	0	(0.00)	1502	(71.05)	1	(0.05)	611	(28.90)	T	3	0	(0.00)	1	(33.33)	0	(0.00)	2	(66.67)
5,969	T	2238	2	(0.09)	80	(3.57)	1	(0.04)	2155	(96.29)	A	1	1	(100.00)	0	(0.00)	0	(0.00)	0	(0.00)
5,978	C	2451	1	(0.04)	2013	(82.13)	1	(0.04)	436	(17.79)	T	1	0	(0.00)	0	(0.00)	0	(0.00)	1	(100.0)

Table 2. Cont.

Nucleo tide Position	LyHCVserumSR										LyHCVpbmcSR									
	Max base	No. of nucleotide	A (%)		C (%)		G (%)		T (%)		Max base	No. of nucleotide	A (%)		C (%)		G (%)		T (%)	
7,172	C	2409	2	(0.08)	1696	(70.40)	1	(0.04)	707	(29.35)	T	3	0	(0.00)	1	(33.33)	0	(0.00)	2	(66.67)
7,274	A	2654	1564	(58.93)	5	(0.19)	1074	(40.47)	11	(0.41)	G	7	3	(42.86)	0	(0.00)	4	(57.14)	0	(0.00)
7,349	G	2510	1019	(40.60)	5	(0.20)	1484	(59.12)	2	(0.08)	A	6	4	(66.67)	0	(0.00)	2	(33.33)	0	(0.00)
7,932	G	2810	1354	(48.19)	0	(0.00)	1453	(51.71)	3	(0.11)	A	9	7	(77.78)	0	(0.00)	2	(22.22)	0	(0.00)
8,093	G	2647	684	(25.84)	3	(0.11)	1956	(73.89)	4	(0.15)	A	7	4	(57.14)	0	(0.00)	3	(42.86)	0	(0.00)
8,168	G	1993	39	(1.96)	1	(0.05)	1952	(97.94)	1	(0.05)	A	2	1	(50.00)	0	(0.00)	1	(50.00)	0	(0.00)
8,237	C	2077	1	(0.05)	2033	(97.88)	0	(0.00)	42	(2.02)	T	3	0	(0.00)	1	(33.33)	0	(0.00)	2	(66.67)
8,672	G	2340	17	(0.73)	576	(24.62)	1734	(74.10)	12	(0.51)	C	3	0	(0.00)	2	(66.67)	1	(33.33)	0	(0.00)
8,693	T	2899	5	(0.17)	690	(23.80)	0	(0.00)	2204	(76.03)	C	3	0	(0.00)	2	(66.67)	0	(0.00)	1	(33.33)

doi:10.1371/journal.pone.0098521.t002

Table 3. Detection of St-Specific HCV-RNA in various kinds of lymphoid cell.

Immune cells	Raji				mir122Raji				Molt-4				naïve T (IL-2)				naïve T (IL6)				naïve T (TGF-β)				naïveT (IL6 and TGF-β)			
HCV-Strain	JFH	HCV	SB	Ly	JFH	HCV	SB	Ly	JFH	HCV	SB	Ly	JFH	HCV	SB	Ly	JFH	HCV	SB	Ly	JFH	HCV	SB	Ly	JFH	HCV	SB	Ly
Positive Strand																												
2 days	1	1	1	1	1	1	1	1	1	1	1	1	1	1	1	1	1	1	1	1	1	1	1	1	1	1	1	1
7 days	0	1	16	4	0	1	64	16	0	1	16	4	0	0	16	4	0	0	4	4	0	0	16	4	0	0	16	4
7 days-UV-irraidated	0	0	0	0	0	0	0	0	0	0	0	0	0	0	0	0	0	0	0	0	0	0	0	0	0	0	0	0
Negative Strand																												
2 days	0	0	1	0	0	0	1	1	0	0	0	0	0	0	1	0	0	0	0	0	0	0	0	0	0	0	0	0
7days	0	0	4	1	0	0	16	4	0	0	4	1	0	0	4	1	0	0	1	1	0	0	4	1	0	0	4	1
7days-UV-irradiated	0	0	0	0	0	0	0	0	0	0	0	0	0	0	0	0	0	0	0	0	0	0	0	0	0	0	0	0

The titers of HCV-RNA were expressed as the highest dilution giving a visible band of the correct size.
Naïve T cells were incubated with IL-1β (10 ng/ml), IL23 (1 ng/ml), and CD3CD28 coated beads.
JFH-1 and HCV-1T are not lymphotropic HCV strains.
SB-HCV and Ly-HCV are lymphotropic HCV strains.
mir122Raji indicate miR122-transduced RIG-1/MDA-knockdown Raji.
doi:10.1371/journal.pone.0098521.t003

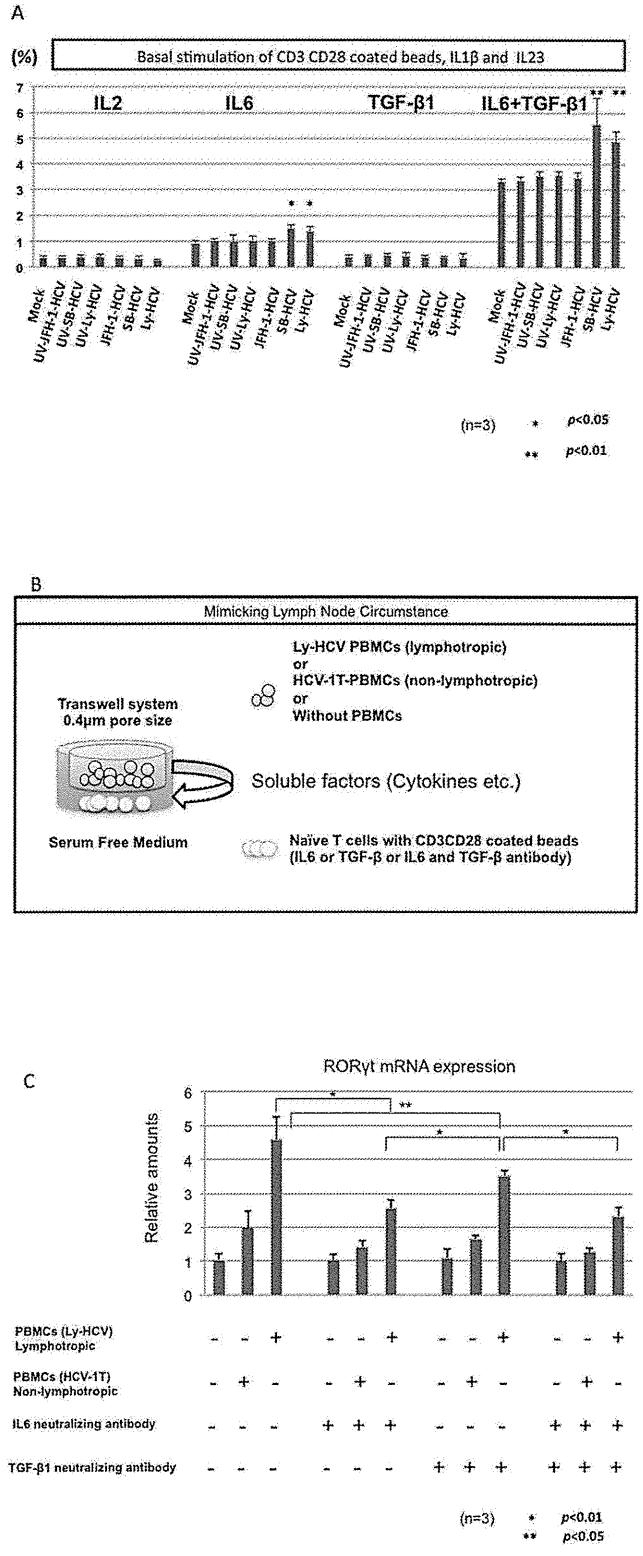

Figure 3. The effect of lymphotropic HCV on the Th17 development in various kinds of cytokines condition. Isolated naïve $CD4^+$ cells were exposed to SB-HCV, Ly-HCV, UV-irradiated-SB-HCV, Ly-HCV or Mock. Then, $CD3^+CD28^+$ coated beads and various kinds of cytokines were added to the culture medium to analyze the Th17 commitment and development (Suppl. Table 1). The cells were harvested at 7 days post-inoculation and IL17A-secreting cells were analyzed by MACS cytokine secretion assay. The frequencies of CD4+ IL17A+ cells among the CD4+ cells were shown in the bar graph (A). The bar graph indicates the frequencies of Th17 cells with or without lymphotropic HCV in the various kinds of cytokine conditions (A). The schema of the transwell system is shown (B). The expression of RORγt mRNA in naïve T lymphocytes with or without various kinds of stimulations is shown (C). The obtained data were analyzed by Mann-Whitney U test. Three independent experiments were carried out (A)(C).
doi:10.1371/journal.pone.0098521.g003

patients were significantly higher than in the other CH-C patients ($p<0.01$) (Fig. 2E). Moreover, these cytokines were significantly correlated with the amount of IL6 and TGF-β1 (data not shown). Then, we quantified the serum cytokines at the twelve months after the Peg-interferon/Ribavirin-treatment among double high patients. The serum amounts of IL-1β, IL17A, IL21 and IL23 were significantly decreased after the achievement of the sustained virological response (SVR) (Fig. 2F).

The relation between lymphotropic HCV and patients with high amounts of IL6 and TGF-β1 (Double-High)

Previously, Machida et al. described that HCV replication in B lymphocytes could induce their secretion of IL6. Therefore, we analyzed the relationship between lymphotropic HCV and patients with double-high by detecting strand-specific HCV-RNA in the $CD4^+$ T cells and $CD19^+$ B cells. The frequency of positive and negative-strand-specific-HCV-RNA in double-high CH-C patients was significantly higher than in the other CH-C patients (Table 1). These data indicated that the lymphotropism of HCV could be related to the IL6 and TGF-β1 double-high environment.

Detection of a new lymphotropic HCV from a patient with lympho-proliferative disease

Previously, we used a lymphotropic SB-HCV that was reported by Sung et al[29]. In this study, we found a patient who had higher amounts of HCV RNA in the lymphocytes in comparison to other CH-C patients. This lymphotropic HCV (named Ly-HCV) is genotype 1b. The full-length sequence of this strain was analyzed by deep sequencing of both serum and PBMC samples. Phylogenetic tree analysis was then carried out (Fig. S1A). To characterize the metagenomics of HCV infection in human serum, LyHCVserumSR (registered in DDBJ; the accession number, AB779562) and PBMC, LyHCVpbmcSR (registered in DDBJ; the accession number, AB779679), we analyzed the samples by paired end deep sequencing. The coverage was 100.0% and the average depth was 2092.1× (Fig. S1B).

The LyHCVserumSR and LyHCVpbmcSR isolates were 99.5% identical to each other within the overlapping region. In 42 nucleotide bases, the major nucleotide bases showed differences. However, only the proportions of nucleotide sequences were different (Table 2). The sequences of HCV-RNA obtained from serum and PBMCs were almost the same (Table 2). Therefore, we used the diluted Ly-HCV-serum for the *in vitro* infection study.

Analysis of Infectivity of Ly-HCV and SB-HCV under the various kinds of cytokines

We examined the infectivity of Ly-HCV and SB-HCV into several lymphoid-cell lines (Raji, miR122-transduced RIG-1/MDA-knockdown Raji, and Molt-4) and primary naïve $CD4^+$ T cells. Semi-quantitative strand-specific nested PCR was carried out as in our previous reports (Table 3). The infectivity of HCV in the IL-6 and TGF-β cytokine combination conditions with low dose IL1β, IL23 and CD3CD28 coated beads was no better than that

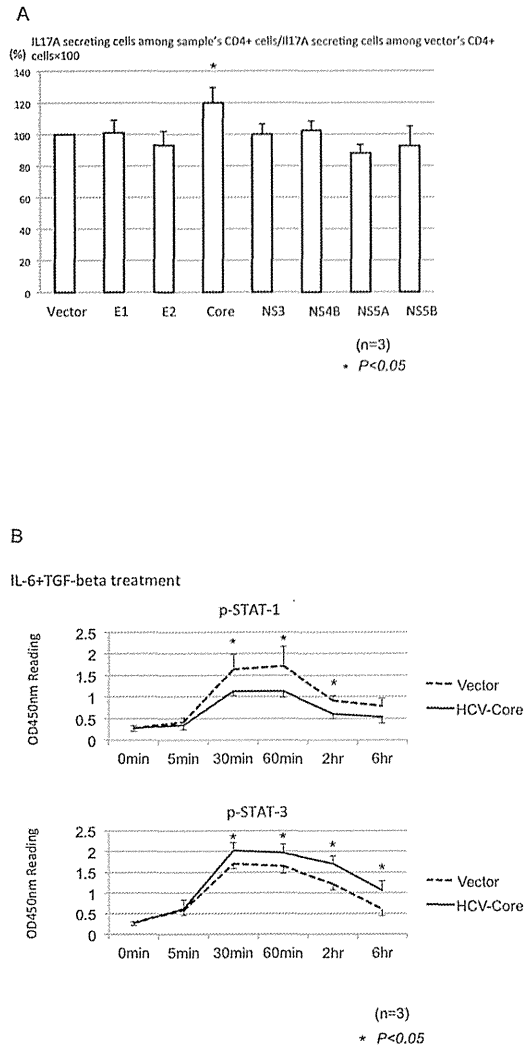

Figure 4. The identification of proteins responsible for enhancing the Th17 development (A). The transfection of various kinds of plasmids expressing HCV-individual proteins (E1, E2, Core, NS3, NS4B, NS5A, NS5B and vector) was carried out by nucleofector. The cells were analyzed at 72 hours post-transfection. The bar graph indicates the IL17A-secreting cells among the sample's $CD4^+$ cells/IL17A secreting cells and the vector's $CD4^+$ cells×100. The obtained data were analyzed by Mann-Whitney U test. Three independent experiments were carried out. **The analysis of STAT-1 and STAT-3 signaling (B).** We used a pathscan to quantify sequentially the phosphor-STAT-1 and STAT-3. The dotted lines indicate data of the vector control. Three independent experiments were carried out. **Long-term culture affected the commitment of naïve T lymphocytes with HCV-core expressing Lenti-virus (C).** The gene expressions of T-bet, GATA-3 and ROR-γt were analyzed by real-time PCR. The relative amounts of mRNA were calculated by ΔΔCT methods. The target gene expressions were analyzed at pre-inoculation of Lent-virus and 10 days after the inoculation of lenti-virus. Three independent experiments were carried out.

doi:10.1371/journal.pone.0098521.g004

in IL2, IL6, or TGF-β cytokine only conditions with low dose IL1β, IL23 and CD3CD28 coated beads.

The effect of lymphotropic HCV on the Th17 development

The addition of both IL6 and TGF-β1 could significantly induce IL17-secreting T cells (Th17) in comparison to IL6 or TGF-β1 alone (Fig 3A). Both lymphotropic HCV strains (SB-HCV and Ly-HCV) could significantly up-regulate the Th17 development in comparison to Mock and these strains that had been UV-irradiated. Then, we used a co-culture system to analyze the blocking of IL6 and TGF-β1 effects since the expressions of IL6 and TGF-β1 mRNA in PBMCs of double high patients were significantly higher than those in other CH-C patients (Fig. 2D and Fig. 3B). The IL-6 was produced from B lymphocytes. Moreover, the major TGF-β1 producing cells were monocytes in double high patients (Data not shown). The soluble factors produced from PBMCs of Ly-HCV-patient could significantly induce Th17 master gene RORγt in comparison to mock and PBMCs of HCV-1T patient (Fig. 3C). The addition of IL6 and TGF-β1 neutralizing antibody significantly reduced the expression of RORγt, especially IL6 neutralizing antibody (Fig. 3C).

The identification of HCV proteins and signal transduction responsible for the production of IL17A

We used E1, E2, Core, NS3, NS4B, NS5A and NS5B expressing plasmids to transiently express these proteins in naïve T cells. The transfection efficiencies were 45.4±4.96% (average±standard deviation). Among these proteins, only HCV-Core protein could significantly enhance the production of IL17A cells (Fig. 4A)($p<0.05$). In addition to in vitro circumstance, we used NOD/scid/γc^{null} (NOG) mice that are super-immunodeficiency mice[33]. The transfusions of HCV-core expressing human primary lymphoid cells were carried out (*ongoing Kondo Y et al.*). The higher amount of IL17A and RORγt mRNA were detected in the HCV-Core expressing $CD4^+$ cells in comparison to the control groups (data not shown). Then, we sequentially analyzed the STAT-1 and STAT-3 activation by IL6 and TGF-β1 stimulation in the HCV-Core expressing T cells. The results indicated that STAT-3 signaling was significantly enhanced in comparison to mock-transfected T cells (Fig. 4B)($p<0.05$). These data indicated that HCV-Core protein enhanced the STAT-3 signaling following the induction of the Th17 master gene-RORγt.